Published in final edited form as:
J Proteome Res. 2011 October 7; 10(10): 4388–4404. doi:10.1021/pr200225c.

Choice of Biological Source Material Supersedes Oxidative Stress in Its Influence on DJ-1 in Vivo Interactions with Hsp90

Christiane B. Knobbe[†,¶], **Timothy J. Revett**[‡,¶], **Yu Bai**[‡,‖], **Vinca Chow**[†], **Amy Hye Won Jeon**[‡], **Christopher Böhm**[‡], **Sepehr Ehsani**[‡], **Thomas Kislinger**[§], **Howard T. Mount**[‡], **Tak W. Mak**[†], **Peter St. George-Hyslop**[‡,⊥], and **Gerold Schmitt-Ulms**[*,‡]

[†]Campbell Family Institute for Breast Cancer Research, Princess Margaret Hospital, University Health Network, Toronto, Ontario M5G 2C1, Canada

[‡]Departments of Laboratory Medicine and Pathobiology, Medical Biophysics, and Medicine (Neurology), Tanz Centre for Research in Neurodegenerative Diseases, University of Toronto, Toronto, Ontario M5S 3H2, Canada

[§]Division of Cancer Genomics and Proteomics, Ontario Cancer Institute, University Health Network, Toronto Medical Discovery Tower, Toronto, Ontario M5G 1L7, Canada

[⊥]Cambridge Institute for Medical Research, University of Cambridge, Cambridge CB2 0XY, U.K

Abstract

DJ-1 is a small but relatively abundant protein of unknown function that may undergo stress-dependent cellular translocation and has been implicated in both neurodegenerative diseases and cancer. As such, DJ-1 may be an excellent study object to elucidate the relative influence of the cellular context on its interactome and for exploring whether acute exposure to oxidative stressors alters its molecular environment. Using quantitative mass spectrometry, we conducted comparative DJ-1 interactome analyses from in vivo cross-linked brains or livers and from hydrogen peroxide-treated or naïve embryonic stem cells. The analysis identified a subset of glycolytic enzymes, heat shock proteins 70 and 90, and peroxiredoxins as interactors of DJ-1. Consistent with a role of DJ-1 in Hsp90 chaperone biology, we document destabilization of Hsp90 clients in DJ-1 knockout cells. We further demonstrate the existence of a C106 sulfinic acid modification within DJ-1 and thereby establish that this previously inferred modification also exists in vivo. Our data suggest that caution has to be exerted in interpreting interactome data obtained from a single biological source material and identify a role of DJ-1 as an oxidative stress sensor and partner of a molecular machinery notorious for its involvement in cell fate decisions.

Keywords

DJ-1; Hsp90; interactome; iTRAQ mass spectrometry; tcTPC

[¶]**Author Contributions**
These authors contributed equally to this work.

[*]**Corresponding Author** Tel: (416) 946-0066. Fax: (416) 978-1878. g.schmittulms@utoronto.ca.
[‖]**Present Addresses**
Beijing National Laboratory for Molecular Sciences, College of Chemistry and Molecular Engineering, Peking University, Beijing, 100871, P. R. China.

Introduction

Human DJ-1, with its 189 amino acids, is a relatively small protein encoded on chromosome 1 (1p36.2-3) of the human genome. The protein is of interest to both cancer and neurodegenerative disease research. More specifically, DJ-1 expression is upregulated in multiple cancers,1,2 and the protein has been implicated in cell fate decisions that influence the invasiveness and metastasis of tumors.3 In the context of neurodegenerative diseases, mutations within DJ-1 have been identified to cause a rare autosomal recessive, early onset PARK7 form of Parkinsonism.4 DJ-1 is part of a diverse superfamily with various clades that contain chaperones, cysteine proteases, and many proteins of unknown function.5 Structural investigations revealed that mature DJ-1 is characterized by a flavodoxin-like Rossmann-fold, largely consisting of a β sheet sandwiched between α helices.6–8 A similar fold has also been observed in other proteins of the DJ-1/ThiJ/Pfpl/Hsp31 superfamily. However, individual superfamily members can be structurally distinguished by specific insertions within the core fold that contribute to a surprising diversity in quaternary oligomerization states.9 Thus, while Pfpl requires assembly into a homohexamer for its putative proteolytic activity,8 the functional form of DJ-1 is expected to predominantly exist as a homodimer. PARK7 mutations that map to DJ-1 may cause a loss of the entire protein or generate loss-of-function versions of this protein,4 possibly by interfering with its homo-dimerization7 or by forming unstable higher order complexes.10

In the brain, DJ-1 has been observed to be widely expressed in cortical areas but is particularly abundant in neurons within the hippocampus, the basolateral amygdala, and the substantia nigra, where it has been reported to localize to both neuronal and nonneuronal cells.11 Originally identified as an oncogene in a mouse fibroblast cell line (NIH 3T3),12 whose ability to transform cells was further potentiated in the presence of ras or myc, the cellular function of DJ-1 has remained enigmatic despite the broad research interest in this protein. Proposed roles include an involvement in transcriptional regulation and/or protective roles as a molecular chaperone in the cellular response to oxidative or chemical stresses. Given a high level of expression of DJ-1 across multiple tissues observed in wild-type mice, it came as a surprise that mice deficient for the DJ-1 gene show no overt phenotype.13 A mild phenotype can be elicited in these mice if they are experimentally exposed to oxidative stressors.14 Also, a mild memory impairment phenotype has been reported in DJ-1-deficient mice, characterized by a reduction in long-term potentiation in the hippocampus. However, no dopaminergic neuronal degeneration or oxidative damage was observed in aged DJ-1-deficient mice.15

A conserved and putatively nucleophilic cysteine residue (Cys106) that may contribute to a catalytic center is buried in the DJ-1 monomer, and it has been suggested that DJ-1 is modified in response to oxidative stressors by oxidation of this Cys106 residue.16 A similar redox biology is well-known to exist in the peroxiredoxin protein family,17,18 an observation that, together with other similarities in size, structure, and putative function, has invoked the characterization of DJ-1 as a peroxiredoxin-related molecule.19

For proteins of unknown function, a characterization of the proteins they partner with can sometimes provide a first step toward elucidating a physiological role. Multiple investigators have taken this direction for DJ-1 and have cumulatively reported more than a dozen putative interactors of DJ-1, which include the protein inhibitor of activated STAT (PIAS) xalpha,20 a largely uncharacterized DJ-1 binding protein (DJBP),21 Daxx,22 parkin,23 α-synuclein,24 Hipk1,25 the androgen receptor,26 histone deacetylase 6 (HDAC6),27 and phosphate and tensin homologue deleted on chromosome 10 (PTEN).28 The most comprehensive analysis of this kind compared the interactomes of DJ-1 and α-synuclein in a rat mesencephalic neuronal cell line in the presence and absence of the pesticide rotenone, known to induce Parkinson's disease-like symptoms in rats.29 The incorporation of quantitative mass spectrometry facilitated the direct comparison of hundreds of proteins that copurified with the baits in that work, including the proteins clathrin, nucleolin, and calnexin, but the absence of a negative control made it difficult to distinguish interactors from unspecific binders. Taken together, little agreement exists regarding the biological significance of currently known DJ-1 interactors.

Given the astonishing range of candidate interactors that the small DJ-1 protein has been proposed to bind directly to in the aforementioned studies, the question arises whether DJ-1 binds to different proteins in diverse cellular contexts and experimental paradigms. Sightings of DJ-1 have been reported in cellular compartments as diverse as the cytoplasm, the mitochondria, and the nucleus, which, assuming these differences are not mere experimental artifacts, may be indicative of an ability of this protein to play a role in diverse subcellular environments.21,30–33 Cumulatively, the above properties make DJ-1 an interesting protein target for interactome investigations designed to (i) address whether this protein exists as a part of a larger protein complex, (ii) elucidate the relative influence of the cellular context (tissue versus cell-based) on its interactome, and (iii) explore whether acute exposure to oxidative stressors alters the molecular environment of DJ-1. Because DJ-1 is a highly abundant protein, an investigation of its molecular neighborhood is likely to reveal other highly abundant proteins. In a situation such as this, the use of quantitative mass spectrometry is indispensable, as many of these highly abundant proteins may also populate protein lists obtained in negative control samples on account of their increased likelihood to either be trapped at a low level in the affinity matrix or to inadvertently copurify because of their dominant presence in cellular extracts. Here, we used two complementary quantitative profiling strategies, the label-free spectral counting method34 or isotopic tagging for relative and absolute quantitation (iTRAQ),35 to address this challenge.

In the following sections we will present glimpses into a biological role of DJ-1 as a molecular neighbor and possible partner of key protein players that are notorious for their involvement in cell fate decisions. The data we present in this article suggest that caution has to be exerted in interpreting interactome data obtained from a single biological source material, in particular for abundant proteins expressed in different cell types and tissues.

Experimental Section

Antibodies

The affinity-purified rabbit anti-DJ-1 antibody we used in this study had been raised against full-length human DJ-1 and is known to be reactive toward rodent and human DJ-1 (SIG-39835, Covance, CA). The Hsp90 antibody (610418, BD Biosciences, NJ) and HSP8A/HSC70 antibody (ab19136, Ab-Cam, MA) are both reactive to the rodent and human isoforms of their respective heat shock protein family members. The antibody reactive to VCP (G-20) is known to react with a sequence located at the C-terminus of human VCP (Santa Cruz Biotechnology Inc., CA). Antibodies directed against Akt (9272, Cell Signaling Technology, Inc., MA) and Raf-1 (C-12, Santa Cruz Biotechnology Inc., CA) recognize mouse and human sequences.

Cell Culture, in Vivo Cross-Linking, Inhibitor, and Oxidative Treatments

Murine homozygous knockout (DJ-$1^{-/-}$) embryonic stem cells were generated by high G418 concentration selection of heterozygous knockout (DJ-$1^{+/-}$) embryonic stem cells for 9 days, followed by the picking, growing up, and screening of single colonies for homozygous deletion of DJ-1. Embryonic stem-cells (wild-type (DJ-$1^{+/+}$), heterozygous (DJ-$1^{+/-}$), and homozygous knockout (DJ-$1^{-/-}$)) were cultured in Dulbecco's Modified Eagle's Medium (DMEM, Gibco) containing 15% (v/v) fetal bovine serum (FBS, Gibco), 1% leukemia inhibitory factor (LIF), 2 mM glutamine, 1% (v/v) penicillin/streptomycin (50 U/mL), and 1 mM β-mercaptoethanol. Where indicated, cells were treated before Western blot analyses for 16 h in the presence or absence of 1 μM of geldanamycin or 150 μM of H_2O_2 before being washed twice in ice-cold phosphate buffered saline and scraped from the dish. Subsequently, proteins were extracted with 1% deoxycholate (DOC), 1% NP-40, and 20 mM Tris, pH 8.3, supplemented with 1× Complete Protease Inhibitor Cocktail (Roche, Palo Alto, CA) before being incubated on ice for 30 min, sonicated for 5 min, and centrifuged at 100000g for 1 h. Protein concentrations of cleared cell lysates were calculated using a bicinchoninic acid assay (BCA). The effect of geldanamycin (GA) inhibitor treatments on cell viability was assessed by the Trypan blue dye exclusion assay. Briefly, 0.4% Trypan blue was gently mixed with trypsinized cells and incubated for 5 min at room temperature. Subsequently, the percentage of viable cells per volume equivalent was determined with the use of a hemocytometer. Alternatively, for the protein extraction for the mass spectrometry analyses, cells were incubated in 500 μM of H_2O_2 for 1 h before being processed for formaldehyde crosslinking as previously described for murine neuroblastoma cells (N2a).36

Time-Controlled Transcardiac Perfusion Cross-Linking

The protocol for time-controlled transcardiac perfusion crosslinking (tcTPC) has been described before.37 Briefly, mice were anesthetized intraperitoneally with Nembutal (sodium pentobarbital), and 0.2 mL of 1000 U/mL heparin solution was also administered to prevent blood clotting. The chest was cut open in a caudal to rostral direction to the sternum, along the sides of the rib cage and secured with either hemostats or retractor forceps. The tip of the heart was secured with forceps then carefully clamped across with a curved hemostat. A slit was cut into the left ventricle, recognizable by its lighter color, into which a 30-mm-long 20-gauge needle with barrel tip, clamped into place with a hemostat and Luer lock hub,

was inserted. The left atrium was cut, and the animal was perfused with saline at 25 mL/min for 2 min to purge the blood vessels. The perfusion was switched to fixative solution at 25 mL/min, and cross-linking was carried out for 6 min, with the absence of blood in the tail and a hardening of the limbs of the animal signaling a successful perfusion. After perfusion, the brain and liver were rapidly removed, postfixed in cross-linking reagent for up to 15 min at room temperature, and immediately frozen by immersion in liquid nitrogen. To increase the throughput of the tcTPC perfusions to 10 per h, individual perfusions were initiated every 6 min in a procedure that required the parallel operation of two peristaltic pumps.

Affinity Purification of Bait Proteins

Approximately 10^9 in vivo formaldehyde (FA)-cross-linked cells of each of the four embryonic stem (ES) cell lines or brain tissue (10 tcTPC-derived brains per sample) were lysed in homogenization buffer (50 mM NH_4Cl, 80 mM Tris, pH 8.0) supplemented with 1× Complete Protease Inhibitor Cocktail (Roche, Palo Alto, CA). To ensure near quantitative extraction of membrane proteins, an equal volume of extraction buffer (20 mM NaCl, 1% sodium deoxycholate, 1% NP-40, 20 mM Tris, pH 8.0) was added, followed by a 30 min incubation on ice and a 5 min sonication in a water bath sonicator. Insoluble cellular and tissue debris was removed by high-speed centrifugation (100 000 g, 1 h). To generate the immunoaffinity matrix, the polyclonal DJ-1-directed antibodies were cross-linked with 20 mM dimethyl pimelimidate (DMP) to protein A agarose (Sigma-Aldrich, Oakville, ON) in the presence of 25 mM Borax, pH 9.4, using standard procedures (30 min, room temperature). Subsequently, the cross-linked bait protein complexes were immunoaffinity-captured on anti-DJ-1 agarose. During this step, samples were gently agitated on a turning wheel for 12 h then washed extensively with 0.5 M NaCl, 0.05% sodium-dodecyl sulfate (SDS), 1% NP-40, 20 mM 4-(2-hydroxyethyl)-1-piper-azineethanesulfonic acid (HEPES), pH 7.3, and detergents were removed by a pre-elution wash with 10 mM NH_4HCO_3, pH 8.0. Proteins were eluted by acidification with 0.2% trifluoroacetic acid, 20% acetonitrile, pH 2.0.

Protein Reduction, Alkylation, and Trypsinization

Protein-containing fractions were denatured in the presence of 6 M urea, 20 mM NH_4HCO_3, pH 8.0, followed by reduction with 1 mM tris-(2-carboxyethyl)-phosphine for 30 min at 60 °C and alkylation with 2.5 mM 4-vinylpyridine for 1 h at room temperature in the dark. To minimize the occurrence of carbamylation, the concentrated urea solution was passed through a mixed-bed ion-exchange resin immediately prior to its use to remove amine-reactive cyanates. Samples were diluted 4-fold to ensure that the concentration of urea did not exceed 1.5 M. Tryptic digestion was initiated by the addition of 1% (w/w) of side chain-modified, L-(tosylamido-2-phenyl) ethyl chloromethyl ketone (TPCK)-treated porcine trypsin and allowed to proceed at 37 °C for 6 h.

iTRAQ Labeling

Following trypsinization, equal quantities of tryptic peptide mixtures were spiked with 1 pmol of synthetic (Glu1)-fibrino-peptide B (GluFib) (Sigma-Aldrich) to serve in the downstream analysis as an internal control for the efficiency of individual labeling reactions. Equal labeling with all four reagents was confirmed by equal intensities of 114:115:116:117

signature peaks upon forced fragmentation of the GluFib $[M + 2H]^{2+}$ parent ion at m/z = 785.85. Any strong deviation from this ratio would have indicated problems with the labeling reaction or recovery of individual samples prior to the sample mixing step. Individual iTRAQ labeling reagents (Applied Biosystems, Foster City, CA) were reconstituted in ethanol, added to peptide mixtures derived from the tryptic digestion of immunoprecipitation (IP) eluates, and incubated at room temperature in the dark for 3 h.

Two-Dimensional Liquid Chromatography

Strong cation exchange (SCX) chromatography was used to achieve peptide fractionation of the complex digest mixture. Samples digested with trypsin were adjusted to 25% acetonitrile and acidified (pH 3.0) by 20-fold dilution in 25% acetonitrile, 20 mM KH_2PO_4, pH 3.0. High-performance liquid chromatography (HPLC) was carried out using the Ultimate System (Dionex, Sunnyvale, CA) equipped with a microflow calibration cartridge, a Valco injection port, and a 180 nL volume UV cell. Separation was achieved on a self-packed 0.5 × 110 mm Luna SCX column (Phenomenex, Torrance, CA) at a flow rate of 18 μL/min with a steep salt gradient from 0–400 mM NH_4Cl in 25% acetonitrile, 20 mM KH_2PO_4, pH 3.0. Fractions eluted from the SCX column were desalted with C18 Empore (3M, Minneapolis, MN) stop and go extraction (STAGE) tips and subsequently subjected to nanoflow reverse-phase (RP)-HPLC using the Ultimate LC system (Dionex, Sunnyvale, CA) equipped with a nanoflow calibration cartridge at a flow rate of 250 nL/min. Peptides were separated on a 75 μm ID self-packed column containing Proteo C12 reverse-phase matrix (Phenomenex) using a 100 min gradient from 2–34% acetonitrile in water, with 0.1% (w/v) formic acid as the ion-pairing agent.

ESI-QqTOF Mass Spectrometry Analysis

The column effluent was coupled directly via a fused silica capillary transfer line to a QSTAR XL hybrid quadrupole/time-of-flight (QqTOF) tandem mass spectrometer (Applied Biosystems; MDS Sciex, Concord, ON, Canada) equipped with a MicroIonSpray electrospray ionization (ESI) source. The progress of each LC–MS run was monitored by recording the total ion current (TIC) as a function of time for ions in the m/z range 300–1800. At 5 s intervals through the gradient, a mass spectrum was acquired for 1 s, followed by one collision-induced dissociation (CID) acquisition of 4 s each on ions selected by preset parameters of the information-dependent acquisition (IDA) method, using nitrogen as the collision gas. Singly charged ions were excluded from CID selection. The collision energy was adjusted automatically for each CID spectrum using an empirically optimized formula that considers the charge state and m/z value of the precursor ion.

Database Searches

Peak lists for database searching were created using Mascot Distiller (Version 1; MatrixScience, London, U.K.). Searches were performed using designated MS/MS data interpretation algorithms within Protein Prospector (Version 4.21.3; University of California, San Francisco, CA)38 and Mascot (Version 2.2; MatrixScience). Searches considered up to one missed cleavage and charge states ranging from +2 to +4. The analysis of iTRAQ data was assisted by the software program ProteinPilot (Version 2.0; Applied Biosystems; MDS Sciex). All proteins listed in the table were identified with confidence by the application of

the following filters: (i) CID spectra with individual confidence scores of less than 80% were not included (the determination of these confidence scores is documented in the Protein Pilot 2.0 Software Help); (ii) assignments to non-iTRAQ-labeled peptides were not considered; and (iii) all identifications of proteins had to be based on at least two CID spectra. The relatively low threshold of 80% was selected so that information that might be of interest to some reader was not lost. Raw iTRAQ ratios were corrected for impurity levels of individual reagent lots determined by the manufacturer. In instances where only two peptides supported the identification of a protein, we required the underlying CID spectra to generate a Mascot score indicating a <5% probability that the match could be considered a random event. It should be noted that the vast majority of proteins were identified with Mascot scores exceeding thresholds conventionally applied for confident identifications. In addition, the proteins that are discussed in greater detail (Hsc70, Hsp90, glycolytic enzymes, and peroxiredoxins) (i) were repeatedly identified with robust scores that exceed conventional confidence thresholds, (ii) were detected by multiple algorithms, and (iii) were indicated to cosegregate with DJ-1 by spectral counting and iTRAQ quantitation. The mass tolerance range between expected and observed masses used for database searches was ±150 ppm for MS peaks and ±0.15 Da for MS/MS fragment ions. Threshold levels were optimized based on LC–MS/MS data sets of tryptic digests of standard proteins. The pyridylethylation of cysteines was expected to occur and, therefore, was considered as a fixed modification during the database queries. The variable modifications carbamylation, N-terminal acetylation or glutamine cyclized to pyroglutamine, oxidation of methionine, and phosphorylation of serines, threonines, or tyrosines were also taken into account when performing database searches. All samples were searched against the International Protein Index (IPI) mouse database at the European Bioinformatics Institute (release from November, 2009) and a “decoy” database in which all entries of the above IPI database had been inverted.

Immunoprecipitation and Western Blotting

Extract proteins were either directly analyzed following the adjustment of protein levels by the bicinchoninic acid method or immunocaptured and eluted in denaturing Laemmli SDS gel loading buffer assisted by incubation at 95 °C for 10 min. Following SDS–PAGE separation on 4–20% Tris–glycine gels, proteins were electrophoretically transferred to poly(vinylidene fluoride) (PVDF) or nitrocellulose membranes. For immunodetection, Western blots were incubated overnight at 4 °C with primary antibodies and for 2 h at room temperature with horseradish peroxidase conjugated secondary antibodies. Protein bands were visualized by enhanced chemiluminescence (ECL).

Results

Quantitative Comparative DJ-1 Interactome Analyses across Selected Tissues

To assess the influence of the cellular environment on the DJ-1 interactome, we initially set out to compare the molecular neighborhood of DJ-1 in alternative tissues: mouse brain versus mouse liver. To stabilize physiological interactions of DJ-1 prior to the disruption of tissue integrity, we employed the tcTPC method. tcTPC exploits the ability of formaldehyde to systemically spread throughout the entire body, pass cellular membranes, and act as a

homo-bifunctional cross-linking reagent for the generation of covalent bonds between proteins which reside in spatial proximity in vivo. Following this step, selected tissues were rapidly dissected and homogenized in the presence of a quenching reagent (ammonium chloride) in order to prevent cross-linking at a time when proteins are no longer present in their physiological microenvironment. To distinguish unspecific binders from specific interactors, we made use of bait exclusion experimental design concepts exploiting the availability of DJ-1 knockout (KO) mice that display no overt phenotype. Thus, homogenates from wild-type (WT) and DJ-1 deficient mouse tissues were side-by-side subjected to coimmunoaffinity purifications. A DJ-1-directed polyclonal antibody was for this purpose covalently immobilized on protein A agarose. Following pH drop elution, proteins were denatured, reduced, alkylated, and trypsinized. To further enable distinction of specific from unspecific interactors and overcome notorious shortcomings posed by the well-known run-to-run variance of highly complex analyte mixtures in mass spectrometry applications, samples were isotopically tagged. More specifically, peptides in negative control samples and specific samples were conjugated to distinct isotopic tags for relative and absolute quantitation (iTRAQ114: negative control DJ-$1^{-/-}$ liver; iTRAQ115: DJ-$1^{+/+}$ liver; iTRAQ, negative control DJ-$1^{-/-}$ brain; iTRAQ117, DJ-$1^{+/+}$ brain). Samples were then combined, fractionated by two-dimensional liquid chromatography (first: strong cation exchange; second: reversed phase), and introduced by electrospray ionization into a quadrupole time-of-flight tandem mass spectrometer. A computational search of the International Protein Index (IPI) mouse database at the European Bioinformatics Institute with masses extracted from collision-induced dissociation (CID) spectra was used to identify candidate proteins cross-linked to DJ-1. Searches against a “decoy database”, in which all sequence entries of the above IPI database were inverted, did not give rise to any protein identification that passed the significance thresholds we had applied; that is, while searches of the decoy database indicated a low false positive rate with which CID spectra were assigned to individual peptides, in no instance could more than one CID spectrum be assigned to the same protein entry in the decoy database. The immunoaffinity purification was repeated once, and only proteins that consistently copurified with the bait were considered (Table 1). The identification of each of these proteins relied on strong CID spectra from at least two peptides. In fact, for each of the 10 most abundant proteins, more than 35% sequence coverage was recorded, and the strongest identification, seen for DJ-1, was based on 36 unique CID spectra and 83.6% sequence coverage. In total, this approach led to the identification of more than 30 proteins that repeatedly passed significance thresholds in consecutive biological repetitions.

The inspection of iTRAQ signature mass peaks that supported the identification of individual proteins revealed the following characteristics: Observed iTRAQ ratios were largely consistent across CID spectra that supported the identification of a single protein. Even when the iTRAQ ratios observed for individual proteins were compared between liver and brain, a high level of correlation was observed, documented by a strong Pearson correlation of 0.847, which, for this sample size, corresponds to a significance level of <0.01 (Figure S3, Supporting Information). However, distinct iTRAQ signature mass distributions could be recognized, which enabled the grouping of proteins into four different candidate categories (Figure 1, Table 1): (I) Tissue-Independent Specific Binder Category: DJ-1 was

the only protein in the list that displayed signal-to-noise of iTRAQ signature mass peak distributions consistent with the interpretation that it was exclusively found in the specific IP samples derived from both brain and liver samples. Also assigned to this category was a small subset of proteins that revealed CID spectra with an iTRAQ distribution that suggested their coenrichment with DJ-1 (e.g., heat shock cognate protein of 70 kDa (HspA8), peroxiredoxins 1 and 6, and glyceraldehyde phosphate dehydrogenase (GAPDH)). However, none of these proteins displayed iTRAQ signature mass peak distributions that suggested exclusive and highly selective coenrichment with DJ-1, as their iTRAQ ratios of 115:114 or 117:116 were consistently lower than the one observed for DJ-1 (please see below for a discussion of this observation). (II) Tissue-Dependent Specific Binder Category: Proteins in this group can be recognized by iTRAQ signature peak distributions characterized by the relative elevation of only one of the DJ-1 specific iTRAQ signature peaks (115 or 117) relative to negative control peaks (114 or 116). Very few proteins appeared to coenrich with DJ-1 in this manner (e.g., syntaxinbinding protein 1, pyruvate kinase, and carbonic anhydrase). Creatine kinase B is a somewhat unusual case in this category, as this protein was essentially nondetectable in the liver. (III) Tissue-Independent Nonspecific Binder Category: A large proportion of proteins were confidently identified on the basis of CID spectra with more or less equal iTRAQ signature mass peaks intensity distributions, arguing that these proteins may have been nonspecifically purified on the affinity matrix (e.g., PACSIN2, valosin-containing protein (VCP)). (IV) Tissue-Dependent Nonspecific Binder Category: Finally, a subset of proteins appeared to have been nonspecifically captured by the affinity matrix in a tissue-dependent manner. Proteins in this group are recognizable by iTRAQ signature peak distributions with similar intensities for brain-derived (114 and 115) or liver-derived (116 and 117) peaks and 117:115 peak intensity ratios that strongly deviate from the value of 1. For example, betaine-homocysteine *S*-methyltransferase-3 and carbamoyl-phosphate synthase were confidently identified in co-IP samples from liver tissue but were essentially undetectable in the brain-derived samples as documented by iTRAQ ratios of 117:115 near 10.

Exemplary Validation of VCP Belonging to Tissue-Independent Nonspecific Binder Category

A strong link exists between VCP and both cancer research and neurodegenerative disease research in the pertinent primary literature (reviewed in refs 39 and 40), which would make this protein a plausible candidate as a DJ-1 interactor. However, the distribution of iTRAQ signature peaks within multiple CID spectra obtained in the above DJ-1 interactome analysis and assigned to this protein suggested that it had merely been nonspecifically copurified with the affinity matrix. To validate this interpretation and, thus, assess in an exemplary fashion the reliability of the iTRAQ assignments, a reciprocal coimmunoprecipitation experiment was performed (Figure S1, Supporting Information). This experiment strongly corroborated the conclusion we had drawn from the distribution of iTRAQ signature peaks, namely, that VCP constitutes a tissue-independent nonspecific binder (category III) to the affinity matrix.

Quantitative Differential DJ-1 Interactome Analysis in ES Cells with and without Oxidative Stimulus

The comparison of DJ-1 brain and liver interactomes suggested that DJ-1 candidate interactors were largely identical in the two different tissues. The fact that each of these tissues is composed of a mixture of cell types suggested that the data we had generated represented the DJ-1 interactome averaged over all of these cell types. To explore to what extent this conceptual choice may have precluded our ability to explore the interactome more deeply, we sought to repeat the DJ-1 interactome analysis with biological material obtained from the expansion of a single cell type. To obtain DJ-1 knockout ES cells, we performed high G418 selection of heterozygous DJ-1 ES cells, which results in the replacement of the wild-type allele by the knockout allele carrying the G418 cassette in a subpopulation of ES cells, which was then expanded after picking and screening individual ES cell colonies. The ease with which a defined cell model is amenable to pharmacological intervention allowed us to further add complexity to the experimental paradigm. Specifically, we wondered whether the interactome of DJ-1 might be less profoundly influenced by cellular context than by oxidative stimuli, which previously had been reported to target DJ-1 to different subcellular compartments. We therefore included in our four-plex analysis a biological sample obtained from the culture of wild-type ES cells subjected to an oxidative stress stimulus exerted by the administration of H_2O_2. As for the previous interactome investigation, all four biological samples were obtained following cross-linking with formaldehyde (Figure 2). Two complementary quantitation strategies were employed in two biological replicates of this experiment to add confidence to interpretations and maximize the number of protein identifications. The spectral counting method was employed for its strength in providing extended coverage of proteins only found in one of the samples that are to be compared, thus minimizing the possibility that a weakly DJ-1-interacting protein may escape detection. iTRAQ-based quantitations were employed because they minimize issues of run-to-run variance, a well-known shortcoming of the spectral counting approach. iTRAQ-based quantitations, however, tend to favor the identification of peptides contributed by more than one of the differentially profiled samples. The computational analyses of the spectral counting interactome data was assisted by ProteinProspector, a suite of algorithms for the mining and interpretation of protein mass spectrometry data. The Search Compare tool within this package allowed the side-by-side comparison of peptides present in the four consecutively generated subdatasets, which were submitted to query the aforementioned IPI database (Table 2). All proteins shortlisted as candidate interactors of DJ-1 on the basis of the spectral counting analysis were present in the eluate fraction derived from DJ-1 heterozygote ES cells with 3–21 CID spectra (corresponding to robust identification scores of 106.1–838.7). In contrast, the same proteins were either entirely absent from eluate fractions derived from DJ-1 knockout ES cells (e.g., HspA8, peroxiredoxin, Hsp90 alpha, Hsp90 beta, and HspA9) or present with spectral counts (and identification scores) that were at least 3-fold lower than the corresponding spectral counts and scores seen in eluates from heterozygote ES cells. The second study, which relied on iTRAQ-based quantitation, was analyzed following the same work-flow described for the liver/brain interactome data. For this data set, CID spectra were analyzed by ProteinPilot (not shown) and Mascot with both algorithms returning essentially identical results (Table 3). Both spectral counting- and iTRAQ-derived DJ-1-interactome data queries

returned DJ-1 as the protein for which the strongest sequence coverage was obtained, indicating success and good yield of the immunoaffinity capture step. A comparison of the two interactome data tables obtained by the two complementary quantitation methods revealed good consistency in the composition and complexity of the interactomes, with more than 30 proteins confidently identified in each of the two samples. A closer comparison of the data sets led to the following observations: (i) A small amount of DJ-1 (~10% seen in the DJ-$1^{+/+}$ interactome) was detected in the interactome derived from the DJ-$1^{-/-}$ ES cells. A subsequent investigation confirmed a small degree of clonal mosaicity in these DJ-$1^{-/-}$ ES cells (not shown), which is a common phenomenon observed after picking ES cell colonies following high G418 selection, as a single remaining heterozygous ES cell may give rise to a persisting heterozygous ES cell subpopulation among an excess of knockout ES cells. The detection of this clonal mosaicity relied strongly on the use of spectral counting because iTRAQ quantitation alone would have suggested at least one alternative interpretation for the appearance of a low-level DJ-1 signal in the negative control sample, namely, a commonly observed minor iTRAQ114 impurity in the iTRAQ115 reagent used for labeling the DJ-1-specific samples. (ii) When analyzed by spectral counting, multiple proteins observed in the DJ-1 interactome derived from ES cells expressing heterozygote or homozygote DJ-1 levels were not detected in the corresponding sample obtained from the DJ-$1^{-/-}$ ES cells (e.g., HspA8, peroxiredoxin-1, Hsp90 alpha and beta) and as such were shortlisted as candidate DJ-1 interactors. (iii) The iTRAQ-based quantitation method pointed at the same proteins; however, instead of a black-or-white result, iTRAQ quantitation made it easier to gauge the relative reduction of these proteins in interactome samples derived from DJ-1-deficient ES cells. (iv) The treatment of wild-type cells with hydrogen peroxide made no difference to the DJ-1 interactome protein lists obtained, arguing that the molecular neighborhood of DJ-1 either remains unchanged under these conditions or physiological changes that do occur cannot be elicited with the methodology we applied.

Comparison of Interactome Data Sets

From a technical point of view, multiple observations suggest that the mass spectrometry analyses produced meaningful data: (i) DJ-1 was consistently ranked as the most prominent hit, both in terms of sequence coverage and in number of unique CID spectra interpreted to be derived from this bait; (ii) several possible technical confounders (e.g., high amount of keratins in samples, low sample quantity, low percentage of isotopic labeling) were not observed; (iii) strong unequivocal assignments of more than 30 proteins could be made per subdataset, and no proteins were identified when peak lists were submitted to decoy database searches.

For the purposes of comparing individual data tables, we decided to sort, in addition to the DJ-1 bait, the strongest candidate interactors in each of the data sets, either on the basis of enrichment ratios that passed the significance threshold of two standard deviations (Figure S2, Supporting Information, iTRAQ data tables) or on the basis of a combination of enrichment ratios and score (spectral counting). As expected, the cutoff values (shown at the bottom of individual data tables) differed, most likely as a consequence of (i) sample-to-sample differences in the iTRAQ mixing ratios of iTRAQ labeled co-IP samples; (ii) DJ-1 levels not being precisely constant across samples, thereby giving rise to different degrees of

enrichment of DJ-1 and its candidate interactors; and (iii) differences in the analysis methods used for quantitation (spectral counting versus iTRAQ). This comparison revealed a considerable overlap, consisting of six of the shortlisted candidate interactors obtained in the ES-based analyses, with those obtained in the DJ-1 brain or liver interactome investigations (Table 4). When we classified candidate interactors according to available gene ontology and functional information, it was apparent that heat-shock proteins, peroxiredoxins, and glycolytic enzymes were overrepresented.

Hsc70 (HspA8) emerged as the most consistent candidate interactor of DJ-1 in this study, observed in both tissues (liver and brain) and in ES cells. The binding of DJ-1 to Hsc70 was specific by three measures: (1) Neither Bip (HspA5) nor HspA2 (Hsp70-3), two other highly abundant cellular chaperones of the Hsp70 family with more than 10 paralogs in humans,41 were found in the data sets. (2) A significant number of other chaperones were found in the sample, but these did not appear to bind to DJ-1, as their presence was undiminished in samples derived from DJ-1 knockout materials. For example, peptides belonging to the mitochondrial chaperones Hsp60 or Hsp10, proteins known to associate with HspA9,42 were found equally distributed in immunoprecipitation eluates collected from DJ-1 knockout and wild-type extracts. (3) Despite the fact that most of the protein mass in eluate fractions was contributed by proteins other than DJ-1, Hsc70 binding was robustly and almost exclusively observed in DJ-1-containing samples. Therefore, only a small fraction of Hsc70 in the respective samples can be attributed to binding of this protein to non-DJ-1 proteins.

Of the total of 16 shortlisted candidate interactors identified (please note that DJ-1 was included in this tally to reflect its well-established ability to dimerize6,8,10), half of them were only found in one of the samples. Importantly, this result cannot simply be ascribed to weak identifications that often underlie run-to-run variance and the sporadic appearance of protein IDs in individual data sets. A case in point is Hsp90 alpha, a protein that was identified as a candidate interactor by ES cell-based DJ-1 inter-actome analyses but not seen in the tissue-based DJ-1 inter-actome data set. Note that in the tissue-derived data set, no CID spectrum was attributed to the presence of Hsp90 alpha (Table 1) despite a robust enrichment of the DJ-1 bait (34 unique CIDs). Contrast this with the 10 unique CID spectra (and a confident Mascot score of 292) that were assigned to Hsp90 alpha in the ES cell-derived data set despite the fact that, based on spectral counts, the latter sample may have contained lesser amounts of DJ-1 (24 unique CIDs) than the tissue-derived IP eluates. Thus, Hsp90 may represent an intriguing example of a protein associated with DJ-1 in ES cells but not in the mouse tissues we investigated.

In Vivo Hydrogen Peroxide Treatment Alters DJ-1 Post-Translational Modification

The DJ-1 literature is divided over whether oxidative stress may lead to changes in the intracellular localization of DJ-1. The interactome data presented in this manuscript suggested that oxidative stress conditions similar to the ones reported to cause cellular redistribution of DJ-1 may not lead to dramatic rearrangements of the next-neighbor relationships that DJ-1 engages in. Naturally, the absence of such an observation could merely reflect an inability of the experimental paradigm to capture these changes or subtle differences of experimental setup that prevent their replication. We therefore explored

alternative means to assess whether DJ-1 was able to “sense” the oxidative stress conditions we had applied in this study through alterations in its post-translational modification state. A subset of previous studies had indicated that oxidative stress may trigger the covalent modification of DJ-1 on amino acid residue Cys106 to cysteine sulfonic or cysteine sulfinic acid.19,43 We therefore edited the MASCOT algorithm to consider three oxidation states of cysteine (cysteine sulfenic, cysteine sulfinic, or cysteine sulfonic acid modifications) in its data analysis. A search of the DJ-1 interactome data set derived from ES cells then confirmed the presence of a strong CID spectrum that assigned a cysteine sulfinic acid modification to the expected amino acid (Figure 3). The confidence of this assignment was corroborated by the following observations: (i) the assignment was highly specific, as no other peptide in the entire data set (out of more than 1000 CID spectra assigned) was interpreted by the algorithm to be modified in this manner, (ii) the search for cysteine sulfonic or cysteine sulfenic acid modifications did not lead to a positive identification, and (iii) the distribution of iTRAQ signature mass peaks within the assigned CID spectrum correlated with the experimental design; that is, whereas the vast majority of CID spectra assigned to DJ-1 showed a distribution of iTRAQ signature mass peaks that indicated relatively equal levels of DJ-1 in eluate fractions (indicated by equal intensities of iTRAQ signature mass peak 115, 116, 117), the CID spectrum which supported the assignment of this modification was primarily contributed by the sample that had been treated with hydrogen peroxide (indicated by iTRAQ signature mass peak 117). Taken together, this experiment confirmed that the oxidative stress conditions these cells had been exposed to had indeed impacted the oxidation state of DJ-1.

DJ-1 Positively Influences the Activity of Mammalian Hsp90

The most striking difference revealed by a comparison of the DJ-1 interactome data obtained from tissue- and cell-based analyses was the absence of Hsp90 from the tissue-based data set. Importantly, both the spectral counting method and the iTRAQ-based quantitation suggested selective coenrichment of Hsp90 with DJ-1 as opposed to an unspecific copurification with the affinity matrix. We therefore decided to explore whether differences in the expression level of Hsp90 in tissue versus ES cells might be responsible for this discrepancy. This turned out not to be the case, as levels of Hsp90 protein observed by Western blotting were highly similar in the selected tissues and ES cells that served as biological source materials in this work (Figure 4). In contrast, peroxiredoxin-1, which was consistently coenriched together with DJ-1 in all coimmunoprecipitations we conducted, appears to be of relatively low abundance in the liver and brain relative to its expression in ES cells. A poor correlate of expression levels and captured amounts of candidate interactors would not be surprising if the expression profiles of DJ-1 and Hsp90 or peroxiredoxin-1 showed little overlap but were counterintuitive for a bait protein as highly and broadly expressed as DJ-1 (see also below). These data further revealed that the absence of DJ-1 does not alter apparent levels of expression of Hsp90 protein. Hsp90 is a widely expressed cellular chaperone, well-known for its role as a key regulator of some of the best-characterized signaling pathways. It is involved in the maturation, stabilization, and/or activation of a select but structurally broad clientele of proteins, including many kinases such as Raf-1 and PKB/Akt. While it has remained largely unknown how Hsp90 acts upon its clients, specific inhibitors such as geldanamycin (GA), a benzoquinone anamycin

antibiotic that binds to Hsp90, have become available.44–46 Consequently, the effect of Hsp90 on kinases can be monitored by employing Western blotting analyses to determine client protein levels, a surrogate frequently used to approximate their relative stabilization. To determine whether DJ-1 might itself be a client of Hsp90 activity or, conversely, whether DJ-1 influences the Hsp90-dependent stabilization of protein levels of a subset of well-established Hsp90 client kinases,47,48 ES cells were subjected to the treatment with GA, and, subsequently, levels of DJ-1, Raf-1, and Akt were assessed by Western blotting following adjustment of protein levels. This experiment revealed no effect of GA on DJ-1 levels and no effect of DJ-1 expression on the GA-dependent inactivation of Hsp90. However, the data robustly demonstrated a positive correlation of the level of Raf-1 or Akt with the level of DJ-1 present in ES cells (Figure 5). We conclude that DJ-1 may act upstream or in concert with Hsp90 as a positive regulator of Hsp90 activity.

Discussion

General Comments

This paper describes large-scale comparisons of the DJ-1 interactomes of in vivo cross-linked mouse brains and livers and of DJ-1 wild-type ES cells. To implement target exclusion concepts and facilitate the recognition of specific candidate interactors from unspecific binders to the affinity matrix, the study made use of DJ-1-deficient mice or mouse embryonic stem cells and complementary quantitative mass spectrometry. Data collected in this work (i) revealed heat shock proteins (HspA8 and Hsp90), peroxiredoxins (1 and 6), and a small number of proteins belonging to the glycolysis pathway in spatial proximity to DJ-1; (ii) established prominent similarities but also striking differences in the interactome data sets of DJ-1 in tissues and cells; (iii) directly documented the in vivo existence of a cysteine sulfinic acid modification of Cys106 within DJ-1 upon exposure of ES cells to hydrogen peroxide stress; and (iv) established Hsp90 as a protein acting downstream or at the level of DJ-1 in a cell-context dependent manner. The results obtained in this work indicate that caution should be exercised when interpreting interactome data obtained from a single biological source.

A particular technical challenge that was represented in this work was the relative abundance of DJ-1 in the cellular proteome. With a protein bait of this nature, it was no surprise that the candidate interactors that emerged from this work were largely known to constitute abundant cellular proteins themselves. We decided to employ in vivo cross-linking to stabilize next-neighbor relationships prior to the disruption of cellular integrity and thus minimize the occurrence of unspecific interactors by enabling stringent washing during subsequent sample handling steps. However, we were cognizant that chemical cross-linking would not only stabilize functional interactions but also generate covalent bonds among proteins which reside in vivo in spatial proximity to each other without necessarily working together in a functional sense. Given the abundance of DJ-1 in the cytosol, it was therefore expected that many highly abundant cytosolic proteins would populate the DJ-1 interactome lists. The situation is further complicated by the notorious representation of some of these highly abundant cytosolic proteins (actin, tubulin, Hsp70, etc.) on interactome data tables of this kind, on account of their tendency to copurify nonspecifically on affinity matrices and

through direct or indirect interactions with other proteins. Spectral counting and iTRAQ-based quantitation data both served the purpose of discriminating specific interactors from unspecific binders and pointing to the same candidate DJ-1 interactors.

Interactome studies of nonabundant bait proteins are often characterized by black-and-white outcomes, with candidate interactors entirely absent from negative control samples. The observation that no DJ-1 candidate interactor that we identified in this work exhibited as high a ratio of enrichment as observed for the DJ-1 bait protein itself was not unexpected and suggests that all candidate DJ-1 interactors were at least in part present in the data sets due to an underlying propensity of these proteins to also bind nonspecifically to the affinity matrix. In this situation, it would be desirable if a threshold could be defined at which a protein can be considered a candidate interactor versus an unspecific binder. Unfortunately, a biologically meaningful threshold cannot be found because the level of enrichment (when comparing specific and negative control sample) could be infinitely small if only a small proportion of a protein engages in a physiological interaction with the bait protein or a sample handling step would disfavor copurification with the bait (e.g., if the cross-linking chemistry employed would not be suited to covalently stabilize an existing interaction). Multiple low abundance cellular proteins were also found in our data set. However, these proteins either were interpreted to have been nonspecifically copurified based on their iTRAQ ratios (e.g., Tim8 and Tim13) or populated the interactome data table at lower ranking positions and therefore were less obvious candidates for followup studies. It is plausible that some of these proteins nevertheless represent biologically important nonstoichiometric interactors of DJ-1, and it is further to be expected that other biologically important interactors were missed, for example, if the conditions of cross-linking and sample processing we had selected did not favor their enrichment or detection. The latter scenario may also have contributed to a low level of overlap of previously reported DJ-1 candidate interactors and interactors identified in this work (restricted to the protein HspA9, see below). Notably though, to our knowledge none of the previously proposed candidate interactors of DJ-1 have been independently confirmed by others and, as such, gained acceptance as authentic DJ-1 interactors at this time.

Sulfinic Acid Modification of Cys106 and Relationship of DJ-1 to Peroxiredoxins

To our knowledge, the identification of the Cys106 sulfinic acid modification represents the first time that this DJ-1 modification was unequivocally confirmed to occur in vivo on the basis of the direct detection of the modified peptide by mass spectrometry. Previous characterizations of DJ-1 protein purified from human umbilical vein endothelial cells initially documented a sulfonic acid modification of this residue.43 However, subsequent high resolution X-ray structure data collected from recombinant DJ-1 favored the interpretation that DJ-1 carries a sulfinic acid modification and suggested that the protein may undergo overoxidation during sample handling steps.49 Most recently, the latter interpretation had gained support from a study that employed sulfinic acid-specific antibodies in order to indirectly assess the oxidation state on this residue.19 The H_2O_2-dependent modification of Cys106 was contrasted by a small, if any, effect of the oxidative stress stimulus on the list of DJ-1 candidate interactors. Upon cursory inspection, this result may contradict previous work that suggested that the oxidation of Cys106 is paralleled by

the relocalization of DJ-1 to mitochondria.30,50 More work will be needed to distinguish between the following plausible interpretations: (1) DJ-1 may not undergo dramatic rearrangements in its interactome or subcellular localization as a result of an oxidative Cys106 modification, (2) DJ-1 may be embedded in a larger protein complex (see below) that relocates to mitochondria, with possibly profound changes of its secondary interactions but little change to direct DJ-1 interactors whose detection is favored in this kind of cross-linking analysis, or (3) only a relatively small proportion of DJ-1 may have shifted in its subcellular location, and the methodology we employed may not be sensitive enough to pick up differences in protein proximities or may be biased against the detection of a subset of interactors.

Peroxiredoxins (Prdxs), a family of ubiquitous peroxidases consisting of six mammalian isoforms, are well-known for a redox chemistry characterized by a redox-active cysteine that can be oxidized to a sulfenic acid51 and, subsequently, recycled to a thiol by, for example, glutathione or ascorbic acid.52 Overoxidation of the respective redox-active cysteines to sulfinic acids has repeatedly been reported and represents a reaction that can be reversed in the presence of sulfiredoxin.53 Our work adds fuel to the hypothesis that DJ-1 itself may constitute an atypical peroxiredoxin-like peroxidase19 by demonstrating that multiple peroxiredoxins coenrich together with the DJ-1 bait in tissue- and cell-based studies. It remains to be shown whether this coenrichment depends on direct interactions with DJ-1 or on an ability to interact with a common binder shared by both DJ-1 and diverse peroxiredoxins (see below). Both peroxiredoxins and DJ-1 occur as structural dimers, and even the existence of disulfide-linked heterodimer intermediates cannot be excluded in light of a report demonstrating an analogous heterodimer structure of peroxiredoxin-6 covalently linked to glutathione S-transferase pi.54

Hsc70 and Hsp90 as Candidate Interactors of DJ-1

It is likely that the Hsc70 binding to DJ-1 was direct (as opposed to mediated through the interaction of DJ-1 with some other protein) because no other protein fulfilled the following two criteria better than Hsc70, that is, gave rise to an equally confident identification (percent sequence coverage) and displayed a stronger dependence on the presence of DJ-1.

Our data do, however, suggest a possible, albeit less prominent, interaction of DJ-1 to at least one other member of the HspA protein family, HspA9, also known as mortalin, which has recently been shown to be substantially decreased in the brains of Parkinson’s disease (PD) patients and in cells treated with the parkinsonian toxicant rotenone.55

A curious observation in this work was the robust but selective coenrichment of Hsp90 with DJ-1 in ES cells but not in mouse tissues. This finding contrasted the consistent coenrichment of Hsc70 with the bait protein. Hsc70, as expected from its designation as a “cognate” member of the Hsp70 protein family, is expressed under basal conditions, whereas Hsp90 is known to be upregulated when cells are placed under certain stress conditions. Though initially attractive as a plausible explanation, upregulation of Hsp90 levels in ES cells seems unlikely as an explanation for the selective coenrichment of Hsp90 in ES cells because expression levels of Hsp90 in samples adjusted for total protein amounts were equal for both tissues and ES cells. The situation is further complicated considering that Hsp90 is

known to work in large chaperone assemblies with possibly over a dozen cofactors that may link it to the proteasome and the Hsc70 system.56 Although some of these cochaperones such as Hsp40 and Hop/Stil have been identified57 and high-resolution structures for individual components of this molecular machinery have become available,58–60 relatively little is known about the molecular architecture of the assembled chaperone machinery or the dynamics of its regulation.

An Emerging Model of DJ-1 in Neurodegeneration and Cancer

This work adds weight to an emerging model, in which key proteins involved in the etiology of Parkinson's disease are constituents of a functionally specialized network, or possibly multiple networks, of protein–protein interactions with Hsc70/Hsp90 chaperones at its core, 61 with Pink1 and Lrrk2 as clients and with direct connections to the proteasome through the interaction of Hsc70 with two ubiquitin 3 ligases, parkin, and the carboxyl terminus of Hsc70-interacting protein (CHIP).62 Possible links of this network to α-synuclein biology have been proposed before63,64 and may involve an interaction of Hsc70 with the cysteine-string protein and small glutamine-rich tetra-tricopeptide repeat-containing protein (SGT). 65,66 In support of a central involvement of the Hsc70/90 chaperone network in Parkinson's disease, (i) Pink1 has been shown to be stabilized by Hsp90;67–69 (ii) LRRK2 has been shown to be stabilized by the carboxyl terminus of CHIP;70–72 (iii) Hsp90 has been shown to regulate recycling of extracellular α-synuclein;73 (iv) parkin has been shown to associate with Hsc7074 and possibly mediate the degradation-independent ubiquitination of Hsc70;75 (v) Hsc70 expression has been documented to prevent α-synuclein-dependent and 1-methyl-4-phenyl-1,2,3,6-tetrahydropyridine (MPTP)-dependent dopaminergic degeneration in Drosophila76 and mouse models77 of Parkinson's disease; (vi) the distribution of the constitutive Hsc70 rather than the inducible Hsp70 has been observed to be altered in PD;78 and (vii) post-mortem Lewy bodies have been shown to immunostain for Hsc70 and Hsp90.79

Do the DJ-1 interactome data presented here shed light on a possible role of DJ-1 in cancer? Our data place DJ-1 within arm's reach of a molecular machinery that connects oxidative stress pathways to PKB/Akt as well as to Ras/Raf-1/MAPK signaling, and one may speculate that these connections are relevant in this context. For instance, the activation of PKB/Akt depends on both the availability of phosphorylated lipids and the support from a specialized Hsp90 chaperone network. The lipid phosphatase and tumor suppressor PTEN, which is known to facilitate the dephosphorylation of 3-phosphoinositide lipid second messengers, especially PtdIns (3,4,5)P_3, and thereby attenuate activation of PKB/Akt, is itself highly susceptible to oxidative stress due to the redox-sensitive cysteines it harbors in its lipid phosphatase catalytic center. The DJ-1 candidate interactor peroxiredoxin-1 has recently been shown to bind to PTEN in a H_2O_2-dependent manner,80 thereby exerting a PTEN protective function. Whereas our own data did not confirm a previously reported direct interaction of DJ-1 and PTEN,3 our data suggest DJ-1 may be able to influence this PTEN inactivation pathway on the basis of its capacity to both bind to peroxiredoxins and absorb H_2O_2 with its oxidation-prone Cys106 residue. The Hsp90-dependent activation of Akt has served as a central paradigm of Hsp90 activity for many years. The robust link of DJ-1 to the Hsc70/Hsp90 molecular network and the demonstration of a reduced

Europe PMC Funders Author Manuscripts

stabilization of Akt in DJ-1 knockout ES cells presented here further strengthen a possible role of DJ-1 in Akt-related cancer pathways.

Conclusion

The data presented in this work are consistent with the notion that DJ-1 acts as a sensor of oxidative stress, possibly in concert with peroxiredoxins and a chaperone network that works to prevent the accumulation of misfolded proteins (Hsc70). Given the appropriate cellular context, a branch of this network may participate in the regulation of signaling pathways (Hsp90) at the intersection of cell fate decisions leading to cellular proliferation (cancer) or cell death (as exemplified in PD).

Supplementary Material

Refer to Web version on PubMed Central for supplementary material.

Acknowledgment

Work on this project was funded through grant support from the Canadian Institutes of Health Research and the Canada Foundation for Innovation. C.B.K was in part supported by a Feodor Lynen Research Fellowship from the Alexander von Humboldt Foundation. G.S.U. received generous support from the W. Garfield Weston Foundation.

Abbreviations

CID	collision-induced dissociation
ESI	electrospray ionization
FA	formaldehyde
GPI	glycosylphosphatidylinositol
HPLC	high-performance liquid chromatography
Hu	human
IP	immunoprecipitation
LC	liquid chromatography
Mo	mouse
MS/MS	tandem mass spectrometry
PD	Parkinson’s disease
PVDF	polyvinylidene fluoride
tcTPC	time-controlled transcardiac perfusion crosslinking

Europe PMC Funders Author Manuscripts

References

(1). Hod Y. Differential control of apoptosis by DJ-1 in prostate benign and cancer cells. J Cell Biochem. 2004; 92(6):1221–1233. [PubMed: 15258905]

(2). MacKeigan JP, Clements CM, Lich JD, Pope RM, Hod Y, Ting JP. Proteomic profiling drug-induced apoptosis in non-small cell lung carcinoma: identification of RS/DJ-1 and RhoGDIalpha. Cancer Res. 2003; 63(20):6928–6934. [PubMed: 14583493]

(3). Kim RH, Peters M, Jang Y, Shi W, Pintilie M, Fletcher GC, DeLuca C, Liepa J, Zhou L, Snow B, Binari RC, Manoukian AS, et al. DJ-1, a novel regulator of the tumor suppressor PTEN. Cancer Cell. 2005; 7(3):263–273. [PubMed: 15766664]

(4). Bonifati V, Rizzu P, van Baren MJ, Schaap O, Breedveld GJ, Krieger E, Dekker MC, Squitieri F, Ibanez P, Joosse M, van Dongen JW, et al. Mutations in the DJ-1 gene associated with autosomal recessive early-onset Parkinsonism. Science. 2003; 299(5604):256–259. [PubMed: 12446870]

(5). Wei Y, Ringe D, Wilson MA, Ondrechen MJ. Identification of functional subclasses in the DJ-1 superfamily proteins. PLoS Comput Biol. 2007; 3(1):e10. [PubMed: 17257049]

(6). Huai Q, Sun Y, Wang H, Chin LS, Li L, Robinson H, Ke H. Crystal structure of DJ-1/RS and implication on familial Parkinson's disease. FEBS Lett. 2003; 549(1–3):171–175. [PubMed: 12914946]

(7). Tao X, Tong L. Crystal structure of human DJ-1, a protein associated with early onset Parkinson's disease. J Biol Chem. 2003; 278(33):31372–31379. [PubMed: 12761214]

(8). Wilson MA, Collins JL, Hod Y, Ringe D, Petsko GA. The 1.1-Å resolution crystal structure of DJ-1, the protein mutated in autosomal recessive early onset Parkinson's disease. Proc Natl Acad Sci U S A. 2003; 100(16):9256–9261. [PubMed: 12855764]

(9). Wilson MA, Ringe D, Petsko GA. The atomic resolution crystal structure of the YajL (ThiJ) protein from *Escherichia coli*: a close prokaryotic homologue of the Parkinsonism-associated protein DJ-1. J Mol Biol. 2005; 353(3):678–691. [PubMed: 16181642]

(10). Macedo MG, Anar B, Bronner IF, Cannella M, Squitieri F, Bonifati V, Hoogeveen A, Heutink P, Rizzu P. The DJ-1L166P mutant protein associated with early onset Parkinson's disease is unstable and forms higher-order protein complexes. Hum Mol Genet. 2003; 12(21):2807–2816. [PubMed: 12952867]

(11). Kotaria N, Hinz U, Zechel S, von Bohlen U, Halbach O. Localization of DJ-1 protein in the murine brain. Cell Tissue Res. 2005; 322:503–507. [PubMed: 16047164]

(12). Nagakubo D, Taira T, Kitaura H, Ikeda M, Tamai K, Iguchi-Ariga SM, Ariga H. DJ-1, a novel oncogene which transforms mouse NIH3T3 cells in cooperation with ras. Biochem Biophys Res Commun. 1997; 231(2):509–513. [PubMed: 9070310]

(13). Goldberg MS, Pisani A, Haburcak M, Vortherms TA, Kitada T, Costa C, Tong Y, Martella G, Tscherter A, Martins A, Bernardi G, et al. Nigrostriatal dopaminergic deficits and hypokinesia caused by inactivation of the familial Parkinsonism-linked gene DJ-1. Neuron. 2005; 45(4):489–496. [PubMed: 15721235]

(14). Kim RH, Smith PD, Aleyasin H, Hayley S, Mount MP, Pownall S, Wakeham A, You-Ten AJ, Kalia SK, Horne P, Westaway D, et al. Hypersensitivity of DJ-1-deficient mice to 1-methyl-4-phenyl-1,2,3,6-tetrahydropyrindine (MPTP) and oxidative stress. Proc Natl Acad Sci U S A. 2005; 102(14):5215–5220. [PubMed: 15784737]

(15). Yamaguchi H, Shen J. Absence of dopaminergic neuronal degeneration and oxidative damage in aged DJ-1-deficient mice. Mol Neurodegener. 2007; 2:10. [PubMed: 17535435]

(16). Kinumi T, Kimata J, Taira T, Ariga H, Niki E. Cysteine-106 of DJ-1 is the most sensitive cysteine residue to hydrogen peroxide-mediated oxidation in vivo in human umbilical vein endothelial cells. Biochem Biophys Res Commun. 2004; 317(3):722–728. [PubMed: 15081400]

(17). Wagner E, Luche S, Penna L, Chevallet M, Van Dorsselaer A, Leize-Wagner E, Rabilloud T. A method for detection of overoxidation of cysteines: peroxiredoxins are oxidized in vivo at the active-site cysteine during oxidative stress. Biochem J. 2002; 366(Pt 3):777–785. [PubMed: 12059788]

(18). Wood ZA, Poole LB, Karplus PA. Peroxiredoxin evolution and the regulation of hydrogen peroxide signaling. Science. 2003; 300(5619):650–653. [PubMed: 12714747]

(19). Andres-Mateos E, Perier C, Zhang L, Blanchard-Fillion B, Greco TM, Thomas B, Ko HS, Sasaki M, Ischiropoulos H, Przedborski S, Dawson TM, et al. DJ-1 gene deletion reveals that DJ-1 is an atypical peroxiredoxin-like peroxidase. Proc Natl Acad Sci U S A. 2007; 104:14807–148122. [PubMed: 17766438]

(20). Takahashi K, Taira T, Niki T, Seino C, Iguchi-Ariga SM, Ariga H. DJ-1 positively regulates the androgen receptor by impairing the binding of PIASx alpha to the receptor. J Biol Chem. 2001; 276(40):37556–37563. [PubMed: 11477070]

(21). Niki T, Takahashi-Niki K, Taira T, Iguchi-Ariga SM, Ariga H. DJBP: a novel DJ-1-binding protein, negatively regulates the androgen receptor by recruiting histone deacetylase complex, and DJ-1 antagonizes this inhibition by abrogation of this complex. Mol Cancer Res. 2003; 1(4): 247–261. [PubMed: 12612053]

(22). Junn E, Taniguchi H, Jeong BS, Zhao X, Ichijo H, Mouradian MM. Interaction of DJ-1 with Daxx inhibits apoptosis signal-regulating kinase 1 activity and cell death. Proc Natl Acad Sci U S A. 2005; 102(27):9691–9696. [PubMed: 15983381]

(23). Moore DJ, Zhang L, Troncoso J, Lee MK, Hattori N, Mizuno Y, Dawson TM, Dawson VL. Association of DJ-1 and parkin mediated by pathogenic DJ-1 mutations and oxidative stress. Hum Mol Genet. 2005; 14(1):71–84. [PubMed: 15525661]

(24). Meulener MC, Graves CL, Sampathu DM, Armstrong-Gold CE, Bonini NM, Giasson BI. DJ-1 is present in a large molecular complex in human brain tissue and interacts with alpha-synuclein. J Neurochem. 2005; 93(6):1524–1532. [PubMed: 15935068]

(25). Sekito A, Koide-Yoshida S, Niki T, Taira T, Iguchi-Ariga SM, Ariga H. DJ-1 interacts with HIPK1 and affects H_2O_2-induced cell death. Free Radical Res. 2006; 40(2):155–165. [PubMed: 16390825]

(26). Tillman JE, Yuan J, Gu G, Fazli L, Ghosh R, Flynt AS, Gleave M, Rennie PS, Kasper S. DJ-1 binds androgen receptor directly and mediates its activity in hormonally treated prostate cancer cells. Cancer Res. 2007; 67(10):4630–4637. [PubMed: 17510388]

(27). Olzmann JA, Li L, Chudaev MV, Chen J, Perez FA, Palmiter RD, Chin LS. Parkin-mediated K63-linked polyubiquitination targets misfolded DJ-1 to aggresomes via binding to HDAC6. J Cell Biol. 2007; 178(6):1025–1038. [PubMed: 17846173]

(28). Kim YC, Kitaura H, Taira T, Iguchi-Ariga SM, Ariga H. Oxidation of DJ-1-dependent cell transformation through direct binding of DJ-1 to PTEN. Int J Oncol. 2009; 35(6):1331–1341. [PubMed: 19885556]

(29). Jin J, Li GJ, Davis J, Zhu D, Wang Y, Pan C, Zhang J. Identification of novel proteins associated with both alpha-synuclein and DJ-1. Mol Cell Proteomics. 2007; 6(5):845–859. [PubMed: 16854843]

(30). Canet-Aviles RM, Wilson MA, Miller DW, Ahmad R, McLendon C, Bandyopadhyay S, Baptista MJ, Ringe D, Petsko GA, Cookson MR. The Parkinson's disease protein DJ-1 is neuroprotective due to cysteine-sulfinic acid-driven mitochondrial localization. Proc Natl Acad Sci U S A. 2004; 101(24):9103–9108. [PubMed: 15181200]

(31). Zhang L, Shimoji M, Thomas B, Moore DJ, Yu SW, Marupudi NI, Torp R, Torgner IA, Ottersen OP, Dawson TM, Dawson VL. Mitochondrial localization of the Parkinson's disease related protein DJ-1: implications for pathogenesis. Hum Mol Genet. 2005; 14(14):2063–2073. [PubMed: 15944198]

(32). Hod Y, Pentyala SN, Whyard TC, El-Maghrabi MR. Identification and characterization of a novel protein that regulates RNA-protein interaction. J Cell Biochem. 1999; 72(3):435–444. [PubMed: 10022524]

(33). Miller DW, Ahmad R, Hague S, Baptista MJ, Canet-Aviles R, McLendon C, Carter DM, Zhu PP, Stadler J, Chandran J, Klinefelter GR, et al. L166P mutant DJ-1, causative for recessive Parkinson's disease, is degraded through the ubiquitin-proteasome system. J Biol Chem. 2003; 278(38):36588–36595. [PubMed: 12851414]

(34). Lundgren DH, Hwang SI, Wu L, Han DK. Role of spectral counting in quantitative proteomics. Expert Rev Proteomics. 2010; 7(1):39–53. [PubMed: 20121475]

(35). Zieske LR. A perspective on the use of iTRAQ reagent technology for protein complex and profiling studies. J Exp Bot. 2006; 57(7):1501–1508. [PubMed: 16574745]

(36). Schmitt-Ulms G, Legname G, Baldwin MA, Ball HL, Bradon N, Bosque PJ, Crossin KL, Edelman GM, DeArmond SJ, Cohen FE, Prusiner SB. Binding of neural cell adhesion molecules (N-CAMs) to the cellular prion protein. J Mol Biol. 2001; 314:1209–1225. [PubMed: 11743735]

(37). Schmitt-Ulms G, Hansen K, Liu J, Cowdrey C, Yang J, DeArmond S, Cohen FE, Prusiner SB, Baldwin MA. Time-controlled transcardiac perfusion crosslinking for the study of protein interactions in complex tissues. Nat Biotechnol. 2004; 22(6):724–731. [PubMed: 15146195]

(38). Chalkley RJ, Baker PR, Medzihradszky KF, Lynn AJ, Burlingame AL. In-depth analysis of tandem mass spectrometry data from disparate instrument types. Mol Cell Proteomics. 2008; 7(12):2386–2398. [PubMed: 18653769]

(39). Vij N. AAA ATPase p97/VCP: cellular functions, disease and therapeutic potential. J Cell Mol Med. 2008; 12(6A):2511–2518. [PubMed: 18798739]

(40). Braun RJ, Zischka H. Mechanisms of Cdc48/VCP-mediated cell death: from yeast apoptosis to human disease. Biochim Biophys Acta. 2008; 1783(7):1418–1435. [PubMed: 18284922]

(41). Tavaria M, Gabriele T, Kola I, Anderson RL. A hitchhiker's guide to the human Hsp70 family. Cell Stress Chaperones. 1996; 1(1):23–28. [PubMed: 9222585]

(42). Deocaris CC, Kaul SC, Wadhwa R. On the brotherhood of the mitochondrial chaperones mortalin and heat shock protein 60. Cell Stess Chaperones. 2006; 11:116–128.

(43). Kinumi T, Kimata J, Taira T, Ariga H, Niki E. Cysteine-106 of DJ-1 is the most sensitive cysteine residue to hydrogen peroxide-mediated oxidation in vivo in human umbilical vein endothelial cells. Biochem Biophys Res Commun. 2004; 317:722–728. [PubMed: 15081400]

(44). Ochel HJ, Eichhorn K, Gademann G. Geldanamycin: the prototype of a class of antitumor drugs targeting the heat shock protein 90 family of molecular chaperones. Cell Stress Chaperones. 2001; 6(2):105–112. [PubMed: 11599571]

(45). Blagosklonny MV. Hsp-90-associated oncoproteins: multiple targets of geldanamycin and its analogs. Leukemia. 2002; 16(4):455–462. [PubMed: 11960322]

(46). Hadden MK, Lubbers DJ, Blagg BS. Geldanamycin, radicicol, and chimeric inhibitors of the Hsp90 N-terminal ATP binding site. Curr Top Med Chem. 2006; 6(11):1173–1182. [PubMed: 16842154]

(47). Sato S, Fujita N, Tsuruo T. Modulation of Akt kinase activity by binding to Hsp90. Proc Natl Acad Sci U S A. 2000; 97(20):10832–10837. [PubMed: 10995457]

(48). Dent P, Jelinek T, Morrison DK, Weber MJ, Sturgill TW. Reversal of Raf-1 activation by purified and membrane-associated protein phosphatases. Science. 1995; 268(5219):1902–1906. [PubMed: 7604263]

(49). Zhou W, Zhu M, Wilson MA, Petsko GA, Fink AL. The oxidation state of DJ-1 regulates its chaperone activity toward alpha-synuclein. J Mol Biol. 2006; 356(4):1036–1048. [PubMed: 16403519]

(50). Blackinton J, Lakshminarasimhan M, Thomas KJ, Ahmad R, Greggio E, Raza AS, Cookson MR, Wilson MA. Formation of a stabilized cysteine sulfinic acid is critical for the mitochondrial function of the Parkinsonism protein DJ-1. J Biol Chem. 2009; 284(10):6476–6485. [PubMed: 19124468]

(51). Claiborne A, Yeh JI, Mallett TC, Luba J, Crane EJ 3rd, Charrier V, Parsonage D. Protein-sulfenic acids: diverse roles for an unlikely player in enzyme catalysis and redox regulation. Biochemistry. 1999; 38(47):15407–15416. [PubMed: 10569923]

(52). Monteiro G, Horta BB, Pimenta DC, Augusto O, Netto LE. Reduction of 1-Cys peroxiredoxins by ascorbate changes the thiol-specific antioxidant paradigm, revealing another function of vitamin C. Proc Natl Acad Sci U S A. 2007; 104(12):4886–4891. [PubMed: 17360337]

(53). Jonsson TJ, Lowther WT. The peroxiredoxin repair proteins. Subcell Biochem. 2007; 44:115–141. [PubMed: 18084892]

(54). Ralat LA, Manevich Y, Fisher AB, Colman RF. Direct evidence for the formation of a complex between 1-cysteine peroxiredoxin and glutathione S-transferase pi with activity changes in both enzymes. Biochemistry. 2006; 45(2):360–372. [PubMed: 16401067]

(55). Jin J, Hulette C, Wang Y, Zhang T, Pan C, Wadhwa R, Zhang J. Proteomic identification of a stress protein mortalin/mthsp70/GRP75: relevance to Parkinson disease. Mol Cell Proteomics. 2006; 5:1193–1204. [PubMed: 16565515]

(56). Saibil HR. Chaperone machines in action. Curr Opin Struct Biol. 2008; 18(1):35–42. [PubMed: 18242075]

(57). Walerych D, Kudla G, Gutkowska M, Wawrzynow B, Muller L, King FW, Helwak A, Boros J, Zylicz A, Zylicz M. Hsp90 chaperones wild-type p53 tumor suppressor protein. J Biol Chem. 2004; 279(47):48836–48845. [PubMed: 15358769]

(58). Ali MM, Roe SM, Vaughan CK, Meyer P, Panaretou B, Piper PW, Prodromou C, Pearl LH. Crystal structure of an Hsp90-nucleotide-p23/Sba1 closed chaperone complex. Nature. 2006; 440(7087):1013–1017. [PubMed: 16625188]

(59). Shiau AK, Harris SF, Southworth DR, Agard DA. Structural analysis of *E. coli* hsp90 reveals dramatic nucleotide-dependent conformational rearrangements. Cell. 2006; 127(2):329–340. [PubMed: 17055434]

(60). Vaughan CK, Gohlke U, Sobott F, Good VM, Ali MM, Prodromou C, Robinson CV, Saibil HR, Pearl LH. Structure of an Hsp90-Cdc37-Cdk4 complex. Mol Cell. 2006; 23(5):697–707. [PubMed: 16949366]

(61). Young JC, Barral JM, Ulrich Hartl F. More than folding: localized functions of cytosolic chaperones. Trends Biochem Sci. 2003; 28(10):541–547. [PubMed: 14559183]

(62). Morishima Y, Wang AM, Yu Z, Pratt WB, Osawa Y, Lieberman AP. CHIP deletion reveals functional redundancy of E3 ligases in promoting degradation of both signaling proteins and expanded glutamine proteins. Hum Mol Genet. 2008; 17(24):3942–3952. [PubMed: 18784277]

(63). Albani D, Peverelli E, Rametta R, Batelli S, Veschini L, Negro A, Forloni G. Protective effect of TAT-delivered alpha-synuclein: relevance of the C-terminal domain and involvement of HSP70. FASEBJ. 2004; 18(14):1713–1715.

(64). Batelli S, Albani D, Rametta R, Polito L, Prato F, Pesaresi M, Negro A, Forloni G. DJ-1 modulates alpha-synuclein aggregation state in a cellular model of oxidative stress: relevance for Parkinson's disease and involvement of HSP70. PLoS One. 2008; 3(4):e1884. [PubMed: 18382667]

(65). Chandra S, Gallardo G, Fernandez-Chacon R, Schlueter OM, Sudhof TC. α-Synuclein cooperates with CSPα in preventing neurodegeneration. Cell. 2005; 123:383–396. [PubMed: 16269331]

(66). Tobaben S, Thakur P, Fernandez-Chacon R, Sudhof TC, Rettig J, Stahl B. A trimeric protein complex functions as a synaptic chaperone machine. Neuron. 2001; 31:987–999. [PubMed: 11580898]

(67). Abeliovich A. Parkinson's disease: pro-survival effects of PINK1. Nature. 2007; 448(7155):759–760. [PubMed: 17700685]

(68). Weihofen A, Ostaszewski B, Minami Y, Selkoe DJ. Pink1 Parkinson mutations, the Cdc37/Hsp90 chaperones and Parkin all influence the maturation or subcellular distribution of Pink1. Hum Mol Genet. 2008; 17(4):602–616. [PubMed: 18003639]

(69). Moriwaki Y, Kim YJ, Ido Y, Misawa H, Kawashima K, Endo S, Takahashi R. L347P PINK1 mutant that fails to bind to Hsp90/Cdc37 chaperones is rapidly degraded in a proteasome-dependent manner. Neurosci Res. 2008; 61(1):43–48. [PubMed: 18359116]

(70). Ding X, Goldberg MS. Regulation of LRRK2 stability by the E3 ubiquitin ligase CHIP. PLoS One. 2009; 4(6):e5949. [PubMed: 19536328]

(71). Hurtado-Lorenzo A, Anand VS. Heat shock protein 90 modulates LRRK2 stability: potential implications for Parkinson's disease treatment. J Neurosci. 2008; 28(27):6757–6759. [PubMed: 18596151]

(72). Ko HS, Bailey R, Smith WW, Liu Z, Shin JH, Lee YI, Zhang YJ, Jiang H, Ross CA, Moore DJ, Patterson C, et al. CHIP regulates leucine-rich repeat kinase-2 ubiquitination, degradation, and toxicity. Proc Natl Acad Sci U S A. 2009; 106(8):2897–2902. [PubMed: 19196961]

(73). Liu J, Zhang JP, Shi M, Quinn T, Bradner J, Beyer R, Chen S, Zhang J. Rab11a and HSP90 regulate recycling of extracellular alpha-synuclein. J Neurosci. 2009; 29(5):1480–1485. [PubMed: 19193894]

(74). Kalia SK, Lee S, Smith PD, Liu L, Crocker SJ, Thorarinsdottir TE, Glover JR, Fon EA, Park DS, Lozano AM. BAG5 inhibits parkin and enhances dopaminergic neuron degeneration. Neuron. 2004; 44(6):931–945. [PubMed: 15603737]

(75). Moore DJ, West AB, Dikeman DA, Dawson VL, Dawson TM. Parkin mediates the degradation-independent ubiquiti-nation of Hsp70. J Neurochem. 2008; 105(5):1806–1819. [PubMed: 18248624]

(76). Auluck PK, Chan HY, Trojanowski JQ, Lee VM, Bonini NM. Chaperone suppression of alpha-synuclein toxicity in a Drosophila model for Parkinson's disease. Science. 2002; 295:865–868. [PubMed: 11823645]

(77). Dong Z, Wolfer DP, Lipp HP, Bueler H. Hsp70 gene transfer by adeno-associated virus inhibits MPTP-induced nigrostriatal degeneration in the mouse model of Parkinson disease. Mol Ther. 2005; 11:80–88. [PubMed: 15585408]

(78). Andringa G, Bol JG, Wang X, Boekel A, Bennett MC, Chase TN, Drukarch B. Changed distribution pattern of the constitutive rather than the inducible HSP70 chaperone in neuromelanin-containing neurones of the Parkinsonian midbrain. Neuropathol Appl Neurobiol. 2006; 32(2):157–169. [PubMed: 16599944]

(79). Uryu K, Richter-Landsberg C, Welch W, Sun E, Goldbaum O, Norris EH, Pham CT, Yazawa I, Hilburger K, Micsenyi M, Giasson BI, et al. Convergence of heat shock protein 90 with ubiquitin in filamentous alpha-synuclein inclusions of alpha-synucleinopathies. Am J Pathol. 2006; 168(3): 947–961. [PubMed: 16507910]

(80). Cao J, Schulte J, Knight A, Leslie NR, Zagozdzon A, Bronson R, Manevich Y, Beeson C, Neumann CA. Prdx1 inhibits tumorigenesis via regulating PTEN/AKT activity. EMBO J. 2009; 28(10):1505–1517. [PubMed: 19369943]

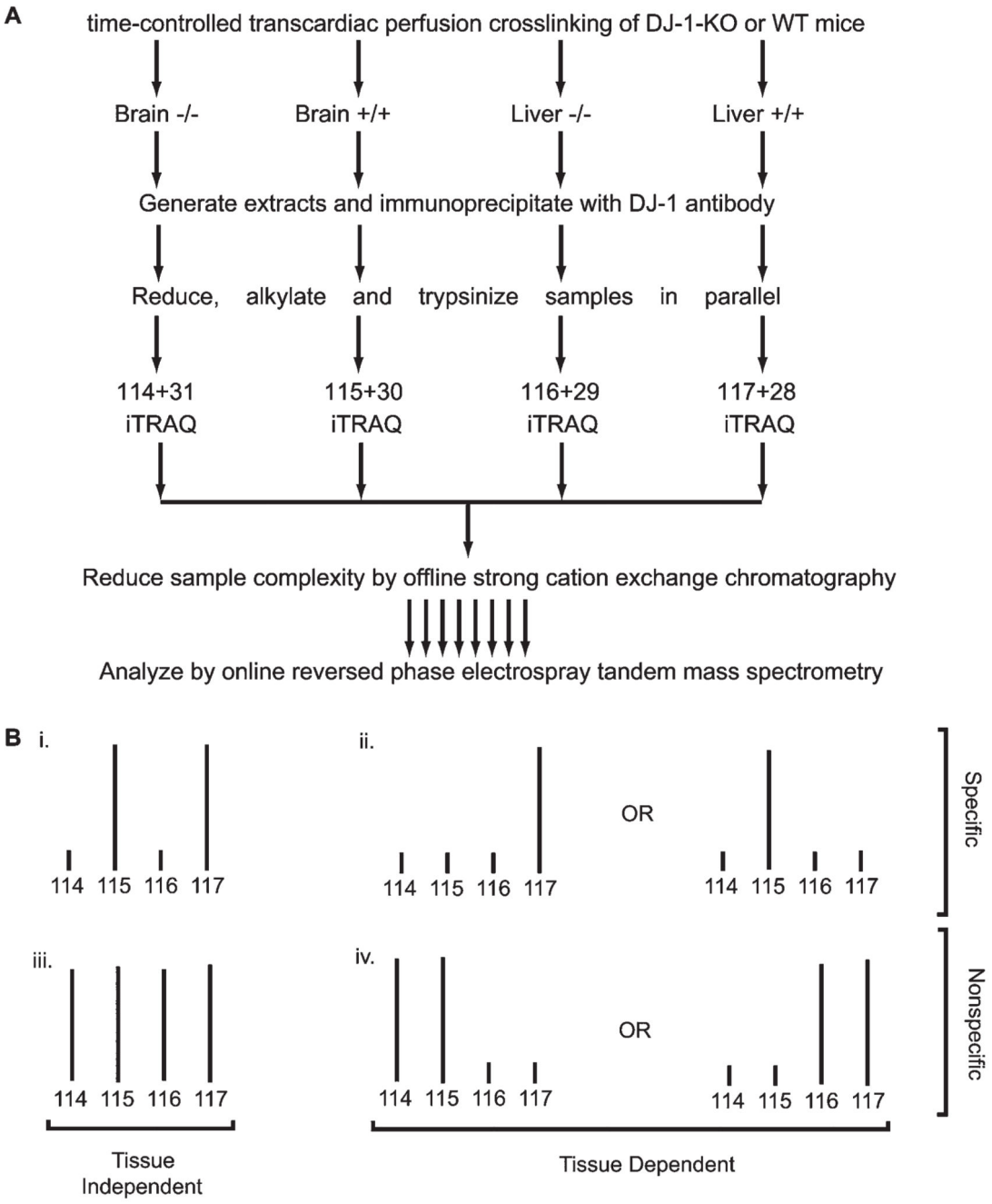

Figure 1.

Quantitative differential profiling strategy employed in this work for the comparison of DJ-1 interactomes from brain and liver. (A) Biological source materials in DJ-1 multiplex interactome comparisons were tissues obtained from wild-type (+/+) or DJ-1 knockout (−/−) mice. Following time-controlled transcardiac perfusion, cross-linking protein complexes were stringently purified with protein A agarose-conjugated antibodies recognizing DJ-1, followed by alkylation and trypsinization. Tryptic sample digests were side-by-side iTRAQ labeled and subsequently combined. Two-dimensional liquid chromatography of peptides

was coupled to online ESI-MS/MS. (B) On the basis of their iTRAQ signature, mass peak ratios of proteins were grouped into four different candidate categories: (i) Tissue-Independent Specific Binder Category, (ii) Tissue-Dependent Specific Binder Category, (iii) Tissue-Independent Nonspecific Binder Category, and (iv) Tissue-Dependent Nonspecific Binder Category. Please note that the assignment to these groups is merely intended to facilitate the grouping of proteins and required the ratio of the respective signature mass peaks to exceed an arbitrarily selected threshold of >3.0.

Europe PMC Funders Author Manuscripts

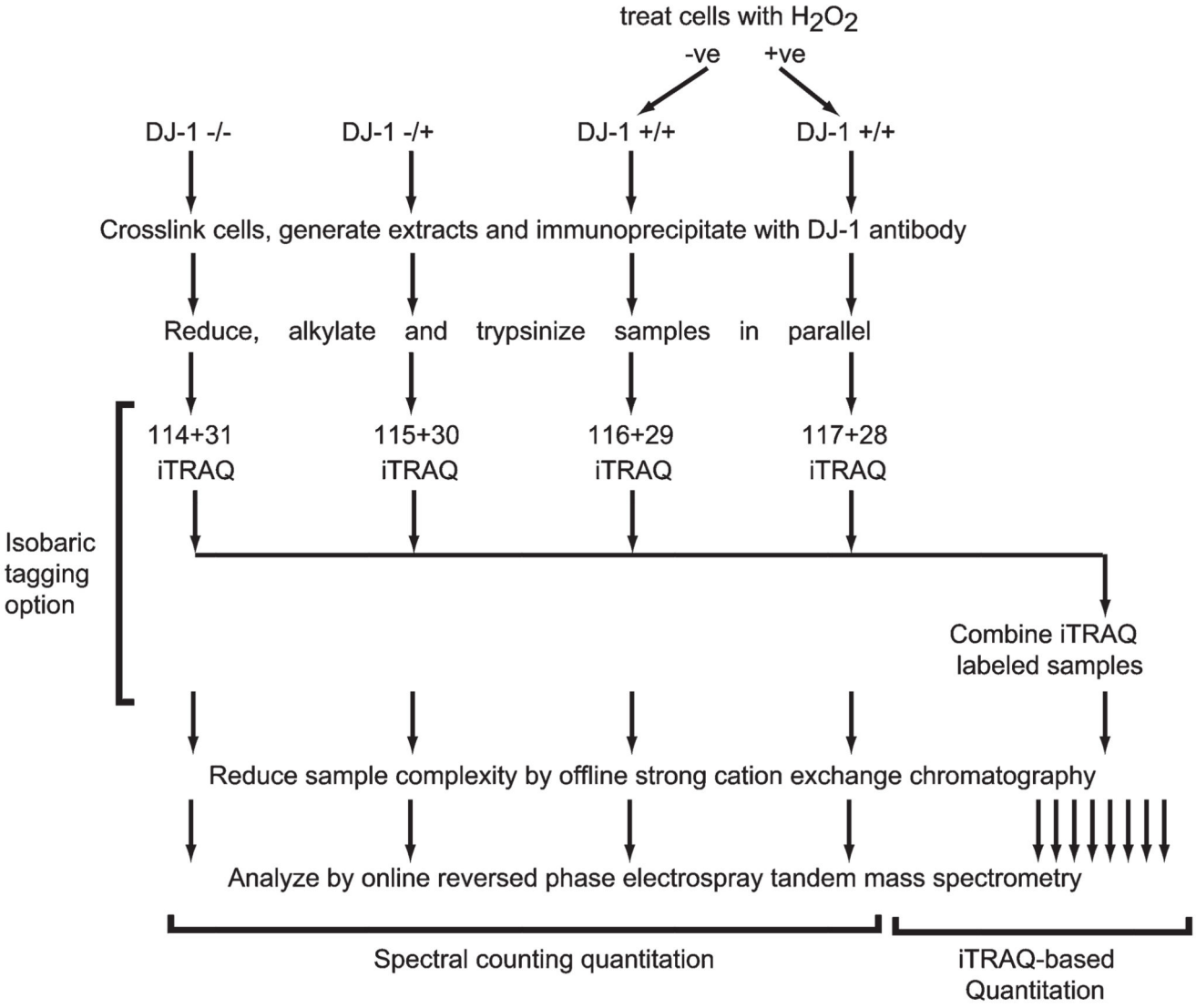

Figure 2.

Alternative strategies used to quantitatively compare DJ-1 interactomes from DJ-1 deficient (−/−), heterozygote (+/−), and wild-type ES cells (+/+) treated with H_2O_2 or untreated. The formaldehyde cross-linking step was achieved by direct addition of the cross-linking solution to adherent cells. Cross-linked protein complexes were stringently purified with protein A agarose conjugated antibodies recognizing DJ-1, followed by alkylation and trypsinization. Tryptic sample digests were either (i) analyzed by consecutive two-dimensional LC, ESI tandem mass spectrometry, and spectral counting quantitation or (ii) side-by-side iTRAQ labeled, subsequently combined, LC fractionated, and analyzed by ESI–MS/MS.

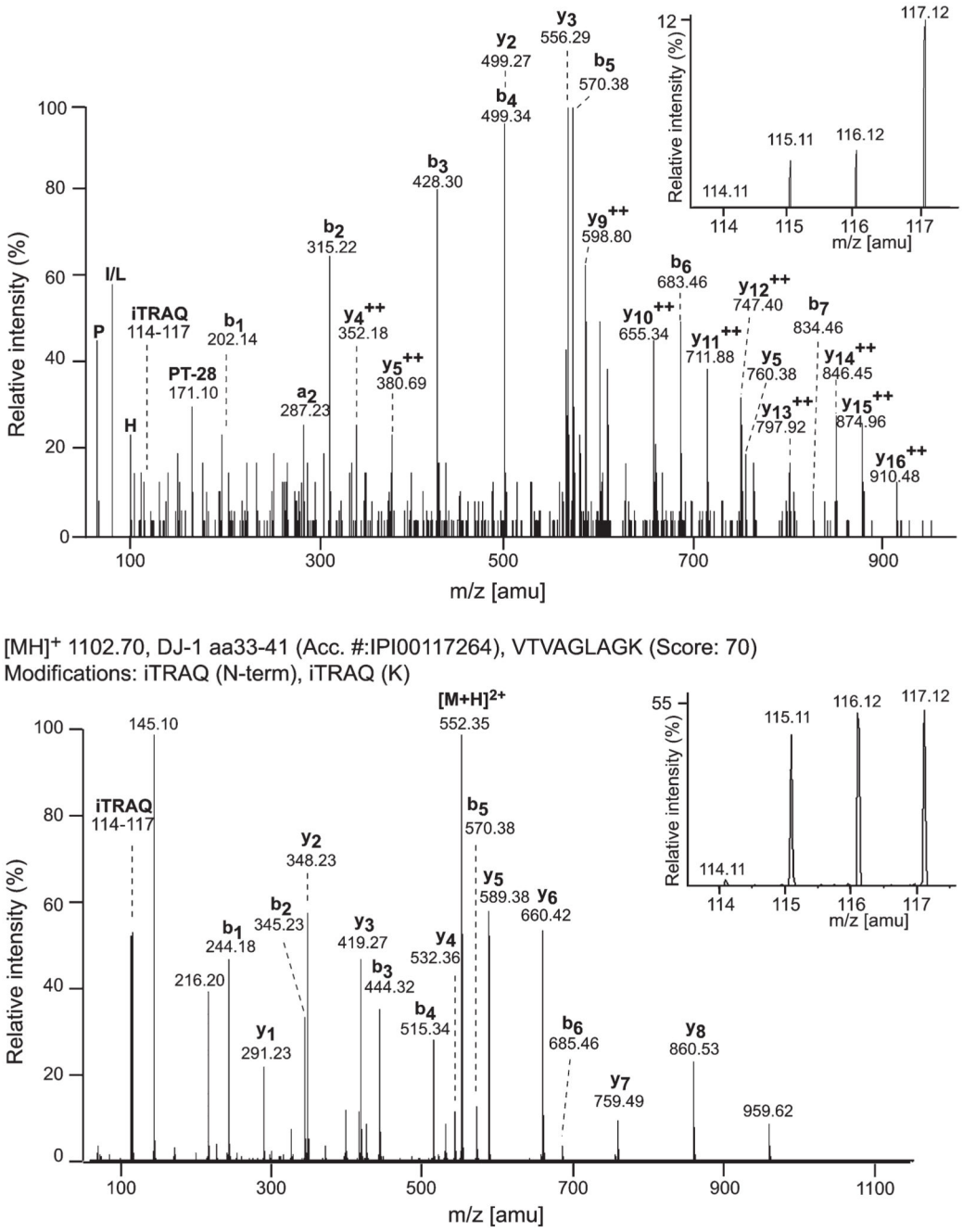

Figure 3.

Direct evidence of DJ-1 Cys106 sulfinic acid modification after H_2O_2 treatment of ES cells. Four-plex comparison of the relative contribution that samples made to the identification of two DJ-1-derived peptides. Parallel co-IPs from DJ-1 deficient, DJ-1 heterozygote, and wild-type ES cells treated or untreated with H_2O_2 were followed by iTRAQ-based quantitation and ESI–MS/MS analyses. iTRAQ labeling reactions were set up as indicated in Figure 3, i.e., iTRAQ114 label: DJ-$1^{-/-}$; iTRAQ115 label: DJ-$1^{-/+}$; iTRAQ116 label: wild-type; and iTRAQ117 label: H_2O_2-treated wild-type ES cells. (A) CID spectrum assigned to tryptic

Europe PMC Funders Author Manuscripts

peptide surrounding the Cys106 residue (GLIAAICAGPTALLAHEVGFGCK). iTRAQ signature mass peak ratios document contribution of this peptide primarily from the H_2O_2-treated wild-type IP eluate, with minor contributions from DJ-1 heterozygote and untreated wild-type ES cells and absence of this peptide in the DJ-1 knockout eluate. (B) Representative CID spectrum assigned to an unmodified DJ-1-derived peptide indicating relatively similar contribution of this peptide from all DJ-1 eluate samples except the negative control. Insets: high resolution graphs depicting iTRAQ signature mass peaks.

Europe PMC Funders Author Manuscripts

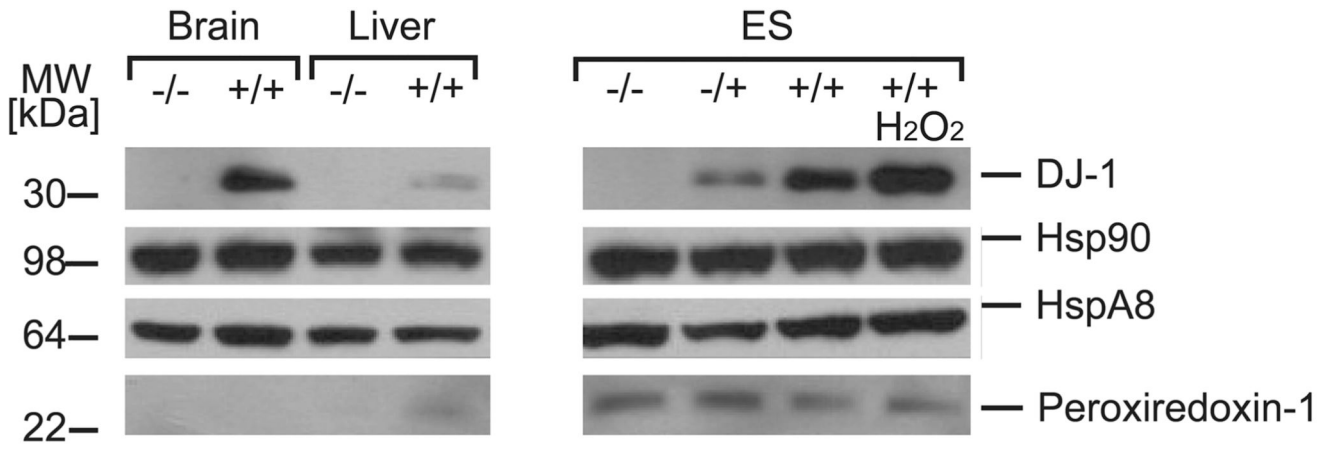

Figure 4.

Expression levels of DJ-1 candidate interactors are a poor predictor for DJ-1 specific coenrichment. Comparison of relative protein levels of DJ-1 and its candidate interactors in different biological source materials. Western blotting analysis using equal protein amounts from brain and liver tissues of DJ-1 knockout and wild-type mice and from DJ-1 knockout, DJ-1 heterozygote, and wild-type ES cells was used to compare the protein levels of a selection of the candidate DJ-1 interactors. Despite the highly selective coenrichment of Hsp90 with DJ-1 only in ES cell-derived samples, similar levels of protein expression can be observed for Hsp90 and Hsc70 (HspA8) in protein extracts derived from brain, liver, and ES cells.

Europe PMC Funders Author Manuscripts

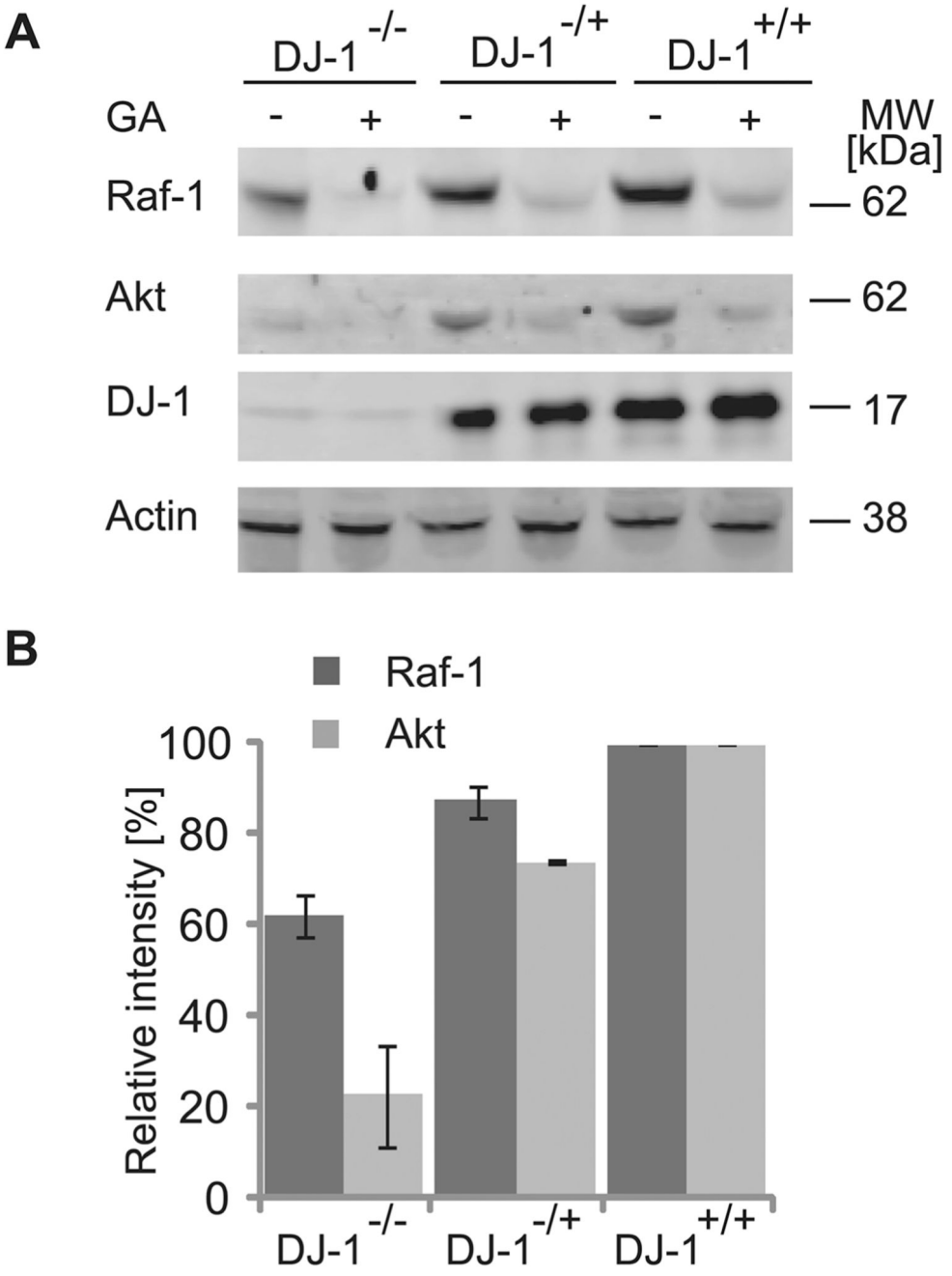

Figure 5.

DJ-1 influences the Hsp90-dependent stabilization of Raf-1 and Akt. (A) DJ-1-deficient, DJ-1 heterozygote, and wild-type ES cells were grown in the presence of carrier solvent or 1 μM of the Hsp90 inhibitor geldanamycin (GA) for 16 h and subsequently analyzed by Western blotting with antibodies directed against DJ-1 or Hsp90-client proteins Raf-1 and Akt. A blot probed with an antibody against actin served as a loading control. Note the absence of an effect of GA treatment on the expression of DJ-1 and the profound increase in Raf-1 and Akt in the presence of DJ-1. (B) Densitometric analyses confirm significant

stabilization of Raf-1 and Akt in DJ-1 expressing cells when compared to DJ-1 knockout. Bar diagram summarizing analyses of three biological replicates of experiment shown in (A) (depicted as percentage of the signals observed for untreated wild-type cells). Differences in Raf-1 and Akt signal levels observed in DJ-1 deficient and DJ-1 expressing ES cells were statistically significant with a *p*-value below 0.05.

Europe PMC Funders Author Manuscripts

Europe PMC Funders Author Manuscripts

Table 1

DJ-1 Candidate Interactors in iTRAQ-Based Four-Plex Comparison of tcTPC Cross-Linked Brain or Liver from DJ-1 KO or WT Mice[a]

					brain		liver						
					KO	WT	KO	WT					
protein name	accession #	MW	unique	% cov	114	115	116	117	115:114	117:116	117:115	114:116	category
DJ-1	**IPI00117264.1**	**20 022**	**34**	**83.6**	**5.3**	**44.3**	**4.8**	**46.6**	**8.4**	**9.8**	**1.1**	**1.1**	**I**
PACSIN2	IPI001 25880.1	55 833	18	56.2	24.3	28.3	22.7	24.7	1.2	1.1	0.9	1.1	III
actin	IPI00110850.1	41 947	11	54.4	20.8	35.1	18.3	25.8	1.7	1.4	0.7	1.1	III
myelin basic protein	IPI00223593.1	20 814	4	51.8	40.2	51.7	3.6	4.5	1.3	1.3	0.1	11.2	IV
argininosuccinate synthase	IPI001 34746.5	46 813	5	44.2	4.5	7.7	44.2	43.6	1.7	1.0	5.7	0.1	IV
Tim13	IPI001 34484.1	10 458	2	42.1	28.5	26.2	31.6	13.7	0.9	0.4	0.5	0.9	III
ATP synthase, alpha	IPI001 30280.1	59 752	4	41.8	18.5	27.7	25.3	28.5	1.5	1.1	1.0	0.7	III
GAPDH	**IPI00849530.1**	**35 679**	**6**	**38.1**	**10.2**	**47.9**	**10.0**	**31.9**	**4.7**	**3.2**	**0.7**	**1.0**	**I**
fructose-bisphosphate aldolase B	**IPI00127206.6**	**39 225**	**8**	**37.4**	**6.7**	**20.5**	**21.0**	**51.8**	**3.1**	**2.5**	**2.5**	**0.3**	**I**
tubulin, beta	IPI001 69463.1	49 832	7	36.6	27.9	49.1	7.6	15.4	1.8	2.0	0.3	3.7	III
tubulin, alpha	IPI00117350.1	49 924	6	36.2	28.1	53.0	8.9	10.0	1.9	1.1	0.2	3.1	IV
VCP	IPI00676914.1	88 852	7	35.6	23.2	29.3	20.7	26.9	1.3	1.3	0.9	1.1	III
Ig gamma-3 chain C region	IPI00117022.2	36 228	5	34.9	22.1	19.9	28.5	29.5	0.9	1.0	1.5	0.8	III
fructose-bisphosphate aldolase A	IPI00856379.1	39 225	3	33.0	28.1	45.7	12.3	13.8	1.6	1.1	0.3	2.3	III
sorbitol dehydrogenase	IPI00753038.1	38 249	3	31.1	5.4	15.3	30.3	48.9	2.8	1.6	3.2	0.2	III
glutathione S-transferase Mu 1	IPI00649450.1	25 969	2	30.4	23.4	20.5	23.4	32.7	0.9	1.4	1.6	1.0	III
V kappa light chain	IPI001 23576.4	12 724	5	30.3	24.6	21.2	24.1	30.1	0.9	1.2	1.4	1.0	III
peroxiredoxin 6	**IPI00758024.1**	**24 826**	**2**	**29.9**	**6.8**	**35.6**	**16.3**	**41.3**	**5.3**	**2.5**	**1.2**	**0.4**	**I**
pyruvate kinase	**IPI00775829.1**	**62 227**	**4**	**29.8**	**4.0**	**15.5**	**29.4**	**51.0**	**3.9**	**1.7**	**3.3**	**0.1**	**II**
betaine-homocysteine S-methyltransferase 3	IPI001 30950.1	45 020	7	29.2	2.1	4.8	43.0	50.1	2.3	1.2	10.4	0.0	IV
enolase, alpha	**IPI00756027.1**	**47 125**	**4**	**28.6**	**12.8**	**47.2**	**11.1**	**29.0**	**3.7**	**2.6**	**0.6**	**1.2**	**I**
HspAS	**IPI00480560.1**	**70 970**	**6**	**28.3**	**14.2**	**44.1**	**8.9**	**32.8**	**3.1**	**3.7**	**0.7**	**1.6**	**I**
superoxide dismutase SOD1	IPI001 30589.7	15 942	2	28.3	7.6	18.1	28.4	45.8	2.4	1.6	2.5	0.3	III
peroxiredoxin-1	**IPI00848536.1**	**18 927**	**4**	**26.8**	**6.0**	**19.1**	**13.9**	**61.0**	**3.2**	**4.4**	**3.2**	**0.4**	**I**
carbonic anhydrase 3	IPI00221890.6	29 366	4	11.8	22.2	14.4	51.5	56.4	0.6	1.1	3.9	0.4	III
Hspa5	IPI00319992.1	72 421	3	26.0	14.5	16.2	30.6	38.7	1.1	1.3	2.4	0.5	III

Europe PMC Funders Author Manuscripts

					brain		liver						
					KO	WT	KO	WT					
protein name	accession #	MW	unique	% cov	114	115	116	117	115:114	117:116	117:115	114:116	category
glutamate dehydrogenase 1	IPI00114209.1	61 337	3	25.6	12.3	24.9	26.7	36.1	2.0	1.3	1.4	0.5	III
syntaxin-binding protein 1	**IPI00415403.1**	**67 569**	**4**	**22.7**	**18.2**	**67.3**	**5.4**	**9.1**	**3.7**	**1.7**	**0.1**	**3.4**	**II**
lactate dehydrogenase	IPI00869393.1	36 368	2	22.7	9.6	16.8	27.5	46.1	1.8	1.7	2.7	0.3	III
ketoacid dehydrogenase E1	IPI00331555.2	50 774	2	21.7	27.4	26.8	18.5	27.3	1.0	1.5	1.0	1.5	III
creatine kinase B-type	IPI00136703.1	42 713	2	21.0	29.6	69.1	1.3	0.0	2.3	0.0	0.0	23.7	IV
Ig gamma-2b	IPI00754836.2	44 561	8	19.3	25.0	27.2	23.5	24.3	1.1	1.0	0.9	1.1	III
phosphoglycerate kinase 1	IPI00555069.3	44 550	3	19.2	10.1	27.3	26.5	36.1	2.7	1.4	1.3	0.4	III
adenosylhomocysteinase	IPI00605533.1	47 585	3	19.0	4.6	9.9	30.7	54.9	2.2	1.8	5.6	0.1	IV
catalase	**IPI00869393.1**	**59 795**	**3**	**16.9**	**9.5**	**13.3**	**22.6**	**54.6**	1.4	**2.4**	**4.1**	**0.4**	**II**
argininosuccinate lyase	IPI00314788.5	55 692	2	13.4	3.2	7.5	29.6	59.8	2.4	2.0	8.0	0.1	IV
carbamoyl-phosphate synthase	IPI00111908.8	166 495	4	12.9	3.0	5.8	29.7	61.5	1.9	2.1	10.6	0.1	IV

[a]Please refer to Table S1 (Supporting Information) for a detailed listing of peptides. DJ-1 candidate interactor significance threshold: (115:114) > 2.8 or (117:116) > 2.2. Please see Figure S2 (Supporting Information), panels A and B, for a graphical depiction of iTRAQ ratios and the calculation of the 95% (two standard deviations) significance threshold. Please refer to the text and Figure 1B for explanations regarding the assignment of proteins to the four classification categories. Data presented in this and subsequent data tables are from one technical replicate.

Europe PMC Funders Author Manuscripts

Table 2

DJ-1 Candidate Interactors in Spectral Counting-Based Comparison of Formaldehyde Cross-Linked DJ-1 KO, HZ, or WT ES Cells with or without H_2O_2[a]

		KO				HZ				WT (−H_2O_2)			WT (+H_2O_2)		HZ/KO
protein name	accession #	MW	score	unique	% cov	score	unique	% cov	score	unique	% cov	score	unique	% cov	score
DJ-1	**IPI00117264.1**	**20 022**	**93**	**4**	**18.5**	**838.7**	**21**	**88.9**	**708.2**	**23**	**88.9**	**424.1**	**16**	**50.8**	**9.0**
Tim8A	IPI00125776.1	11 043	124.4	3	52.6	114.6	3	52.6	51.9	2	22.7	42	1	11.3	0.9
Tim13	IPI00134484.1	10 458	133.4	3	43.2	144.7	3	43.2	66.7	2	26.3	53.2	2	28.4	1.1
10 kDa heat shock protein, mitochondrial	IPI00263863.7	10 832	111.2	4	38.6	131.7	4	38.6	42.4	2	16.8	83.6	3	26.7	1.2
tubulin, beta	IPI00117352.1	49 671	192.4	5	13.7	370.9	11	32.9	82.7	3	9.0	145.6	6	17.8	1.9
CPN10-like protein	IPI00120045.1	10 978	82.3	3	31.4	105.1	3	31.4	24.1	1	9.8	64.5	2	19.6	1.3
60S ribosomal protein P2	IPI00139795.2	11 651	89.5	3	31.3										
GAPDH	**IPI00273646.8**	**35 679**	**85.6**	**3**	**7.8**	**256.2**	**7**	**30.1**	**83.3**	**4**	**13.3**	**117.7**	**5**	**25.0**	**3.0**
HspAS	**IPI00323357.3**	**70 872**				**249.3**	**9**	**21.5**	**277.2**	**13**	**23.1**	**307.6**	**14**	**26.2**	
60 kDa heat shock protein, mitochondrial	IPI00308885.5	60 956	258.6	7	13.3	351.6	9	23.4	128.7	7	13.1	127.6	6	8.7	1.4
peroxiredoxin-1	**IPI00121788.1**	**22 177**				**162.6**	**5**	**23.1**	**19.6**	**1**	**4.0**				
PACSIN2	IPI00125880.1	55 833	308.7	9	19.0	310.8	9	19.8	224.5	10	22.8	161.7	7	14.2	1.0
actin, cytoplasmic 1	**IPI00110850.1**	**41 737**	**33.1**	**1**	**2.9**	**139.1**	**5**	**12.5**	**119.8**	**5**	**14.1**	**159.6**	**7**	**20.0**	**4.2**
ADP/ATP translocase 2	IPI00127841.2	32 800	50.4	2	5.7	85.6	4	12.1	99.1	5	15.2	86.8	4	19.9	1.7
60S ribosomal protein L12	IPI00338838.3	17 793	86.5	2	15.2				21.1	1	5.5				
tubulin alpha	IPI00403810.2	49 910	183.5	5	13.4	75	3	7.8	119.6	5	13.4	122.4	5	13.8	0.4
elongation factor 1-alpha 1	**IPI00307837.4**	**50 314**	**39.5**	**1**	**2.4**	**177.8**	**6**	**13.8**	**99.9**	**5**	**9.5**	**112.5**	**4**	**10.3**	**4.5**
YME1L1	IPI00136555.1	80 029	205.7	8	12.2	239.2	8	11.5	133.1	7	9.0	79.1	4	5.6	1.2
prohibitin	IPI00133440.1	29 820	116.7	3	12.1	26.9	1	4.4	19.4	1	3.7	20.2	1	5.9	0.2
HSP 90, beta	**IPI00554929.1**	**83 195**				**231.2**	**7**	**11.5**	**69**	**3**	**4.0**	**97.2**	**4**	**5.8**	
peptidyl-prolyl cys-trans isomerase A	IPI00554989.1	17 840				68.7	2	11.0	21.9	1	5.5	43.7	2	11.0	
pyruvate kinase	IPI00407130.3	58 004	49.3	2	7.7	108.4	5	10.3				43.2	2	4.1	2.2
actin, gamma	IPI00266875.5	42 880				82.8	3	7.4	46.5	2	4.6	78.8	4	10.2	
ketoacid dehydrogenase E1, alpha	IPI00331555.2	50 774				82.3	3	9.6							
eukaryotic initiation factor 4A-I	IPI00118676.3	46 154	26.8	1	3.9	123.1	4	8.6							4.6
peroxiredoxin-4	IPI00116254.1	31 053	23	1	5.5	61.9	2	6.9	19.6	1	2.9				2.7

Europe PMC Funders Author Manuscripts

		KO				HZ				WT (−H_2O_2)			WT (+H_2O_2)		HZ/KO
protein name	**accession #**	**MW**	**score**	**unique**	**% cov**	**score**	**unique**	**% cov**	**score**	**unique**	**% cov**	**score**	**unique**	**% cov**	**score**
fructose-bisphosphate aldolase A	IPI00221402.6	39 225				41.8	1	3.9	18.4	1	2.5	53.1	2	6.3	
HspA9	**IPI00133903.1**	**73 529**				**120.9**	**3**	**5.9**	**47.2**	**2**	**3.5**				
ATP synthase, alpha	IPI00130280.1	59 753	34.4	1	1.8	73.4	2	4.0	71.7	3	5.2	67.1	2	4.0	2.1
HSP 90, alpha	**IPI00330804.3**	**84 657**				**106.1**	**3**	**4.8**	**69**	**3**	**4.0**	**54.7**	**2**	**3.1**	
enolase 1, alpha	IPI00756027.1	47 125				68.1	2	4.1				28.6	1	2.8	

[a]Please see Table S2 (Supporting Information) for details. DJ-1 candidate interactor filter and threshold: (HZ score > 100) and (HZ score/KO score) > 3.

Table 3

DJ-1 Candidate Interactors in Four-Plex iTRAQ-Based Comparison of Formaldehyde Cross-Linked DJ-1 KO, HZ, or WT ES Cells with or without H_2O_2[a]

						KO	HZ	WT (−H_2O_2)	WT (+H_2O_2)	HZ/KO
protein name	accession #	MW	score	unique	% cov	114	115	116	117	115:114
DJ-1	**IPI00117264.1**	**20 022**	**676.2**	**24**	**54.0**	**3.1**	**29.4**	**31.5**	**35.9**	**9.5**
10 kDa heat shock protein, mitochondrial	IPI00263863.7	10 832	152.8	5	50.5	22.0	31.6	23.9	22.4	1.4
Tim13	IPI001 34484.1	10 458	122.2	3	36.8	43.9	27.3	19.3	9.5	0.6
GAPDH	**IPI00474610.3**	**35 679**	**329.1**	**11**	**27.1**	**12.5**	**31.0**	**27.7**	**28.8**	**2.5**
prohibitin-2	IPI00321718.4	33 297	213.4	9	26.8	32.3	23.4	26.1	18.1	0.7
pubulin, beta	IPI001 69463.1	49 832	379.4	11	26.7	21.2	29.8	24.6	24.5	1.4
Tim8A	IPI001 25776.1	11 043	67.4	2	22.7	51.7	19.6	13.5	15.2	0.4
pibosomal protein L21	IPI00378437.3	18 503	76.0	4	22.5	27.5	24.4	31.1	17.1	0.9
ADP/ATP translocase 2	IPI00127841.2	32 800	192.4	10	21.5	17.7	24.9	27.6	29.7	1.4
PACSIN2	IPI001 25880.1	55 833	410.8	17	21.2	24.9	25.4	26.8	23.0	1.0
actin, alpha	IPI00480406.1	41 947	210.1	9	21.2	16.9	22.8	31.6	28.7	1.3
enolase, alpha	**IPI00462072.2**	**47 010**	**177.8**	**9**	**20.8**	**15.2**	**37.2**	**21.3**	**26.4**	**2.5**
HspA8	**IPI00753407.1**	**76 511**	**456.9**	**15**	**19.8**	**7.0**	**29.4**	**31.3**	**32.3**	**4.2**
fructose-bisphosphate aldolase A	IPI00221 402.6	39 225	168.9	8	19.8	15.0	33.1	25.2	26.6	2.2
ketoacid dehydrogenase E1, beta	IPI00115302.3	35 505	120.0	6	19.3	22.8	25.6	27.4	24.2	1.1
heat-shock protein beta-1	IPI001 28522.1	23 014	89.2	3	16.3	23.7	23.4	26.5	26.4	1.0
ketoacid dehydrogenase E1, alpha	IPI00331 555.2	50 774	162.7	6	15.7	21.2	26.8	28.9	23.1	1.3
peroxiredoxin-1	**IPI00648105.1**	**18 927**	**95.1**	**3**	**14.7**	**12.3**	**30.9**	**28.5**	**28.3**	**2.5**
eukaryotic initiation factor 4A-I	IPI00118676.3	46 154	188.0	5	14.5	18.8	32.9	22.2	26.1	1.7
interleukin-2 precursor	IPI00115183.1	19 400	168.7	6	14.2	21.7	30.5	20.8	27.0	1.4
tubulin, alpha	IPI00117350.1	49 925	150.4	6	14.1	21.3	28.1	24.7	26.0	1.3
YME1L1	IPI001 36555.1	80 029	385.4	11	14.0	23.6	26.3	25.5	24.5	1.1
T-complex protein 1 subunit beta	IPI00320217.8	57 347	159.1	7	13.7	24.8	25.8	25.0	24.5	1.0
60S ribosomal protein L27a	IPI00553612.2	16 458	54.5	2	12.9	23.9	20.9	32.2	23.0	0.9
Hsp 90, alpha	**IPI00330804.3**	**84 657**	**292.3**	**10**	**12.4**	**12.1**	**30.8**	**28.4**	**28.7**	**2.5**
myozenin-3	IPI001 53879.1	26 982	158.1	7	11.8	24.6	29.9	20.4	25.1	1.2
ATP synthase beta chain, mitochondrial	IPI00468481.2	56 301	134.1	5	11.3	20.5	28.2	28.7	22.6	1.4
HspA9	IPI00133903.1	73 529	222.1	10	10.9	15.6	29.1	37.1	18.2	1.9
malate dehydrogenase 2, NAD	IPI00331 590.1	35 612	73.2	3	10.7	22.3	26.2	27.6	23.9	1.2
L-lactate dehydrogenase A chain	**IPI00319994.5**	**36 368**	**69.2**	**3**	**10.6**	**13.3**	**38.3**	**27.9**	**20.5**	**2.9**
elongation factor 1-alpha 1	IPI00307837.4	50 314	134.2	6	10.1	13.6	28.3	25.5	32.6	2.1
60 kDa heat shock protein, mitochondrial	IPI00461 249.1	61 055	146.8	7	9.6	24.0	28.0	24.1	23.9	1.2
Mtap7 protein	IPI00380510.1	82 840	55.1	3	9.6	24.1	26.5	26.8	22.7	1.1
kininogen-1	IPI00114958.1	73103	106.9	5	9.2	22.9	35.7	21.2	20.2	1.6
pyruvate kinase	**IPI00407130.3**	**58 004**	**94.8**	**6**	**9.2**	**12.2**	**37.9**	**23.5**	**26.4**	**3.1**
VCP	IPI00676914.1	88 852	169.2	6	8.9	25.4	22.8	25.9	25.8	0.9
T-complex protein 1, zeta	IPI00116281.2	57 874	102.8	4	8.9	22.1	26.6	26.7	24.6	1.2

						KO	HZ	WT (−H_2O_2)	WT (+H_2O_2)	HZ/KO
protein name	**accession #**	**MW**	**score**	**unique**	**% cov**	**114**	**115**	**116**	**117**	**115:114**
inosine-5′-monophosphate dehydrogenase 2	IPI00323971.2	55 816	65.8	3	8.2	14.0	30.0	28.0	27.9	2.1
ribosomal protein L10	IPI00340103.1	24 558	56.0	3	7.5	25.7	22.1	32.1	20.2	0.9
ubiquitin C	IPI00458995.2	99 577	134.8	6	7.4	20.7	22.6	28.7	28.0	1.1
stress-induced-phosphoprotein 1	**IPI00121514.3**	**62 583**	**47.7**	**2**	**6.1**	**14.2**	**49.7**	**16.5**	**19.6**	**3.5**

[a]Please refer to Table S3 (Supporting Information) for a detailed listing of peptides. DJ-1 candidate interactor filter and threshold: (HZ score: KO score) > 2.4. Please see Figure S2C (Supporting Information) for a graphical depiction of iTRAQ ratios and the determination of the 95% (two standard deviations) significance threshold.

Table 4

Relative Rankings of Short-Listed Candidate Interactors in DJ-1 Interactome Data Sets[a]

		relative rankings			
		brain	liver	ES	ES
candidate interactor class	protein name	iTRAQ	iTRAQ	spectral counting	iTRAQ
bait	DJ-1	1	1	1	1
peroxiredoxins	peroxiredoxin-1	7	2	3	8
	peroxiredoxin 6	2	7		
Hsps	HspA8	9	3	2	2
	HSP 90, alpha			6	9
	HSP 90, beta			4	
	HspA9			5	
	stress-induced-phosphoprotein 1				3
glycolytic enzymes	GAPDH	3	4	9	6
	fructose-bisphosphate aldolase B	8	6		
	pyruvate kinase	4			4
	enolase, alpha	5	6		7
	L-lactate dehydrogenase A chain				5
other	actin, cytoplasmic 1			8	
	elongation factor 1-alpha 1			7	
	syntaxin-binding protein 1	6			
	catalase		8		

[a]Rankings of proteins were derived from their enrichment ratios shown in Tables 1–3. For iTRAQ-based quantitation data, only DJ-1 candidate interactors are shown that passed the significance threshold (enrichment ratio exceeded two standard deviations) depicted in Figure S2 (Supporting Information).